

Can we reconcile the TA excess and hotspot with Auger observations?

Noemie Globus¹, Denis Allard², Etienne Parizot², Cyril Lachaud², Tsvi Piran¹

ABSTRACT

The Telescope Array (TA) shows a 20° hotspot as well as an excess of UHECRs above 50 EeV when compared with the Auger spectrum. We consider the possibility that both the TA excess and hotspot are due to a dominant source in the Northern sky. We carry out detailed simulations of UHECR propagation in both the intergalactic medium and the Galaxy, using different values for the intergalactic magnetic field. We consider two general classes of sources: transients and steady, adopting a mixed UHECR composition that is consistent with the one found by Auger. The spatial location of the sources is drawn randomly. We generate Auger-like and TA-like data sets from which we determine the spectrum, the sky maps and the level of anisotropy. We find that, while steady sources are favoured over transients, the probability to account for all the currently available observational data is very low ($\sim 0.1\%$). While we reproduce fairly well the Auger spectrum for the vast majority of the simulated data sets, most of the simulated data sets with a spectrum compatible with that of TA (at most a few percent depending on density model tested) show a much stronger anisotropy than the one observed. We find that the rare cases in which both the spectrum and the anisotropy are consistent require a steady source within ~ 10 Mpc, to account for the flux excess, and a strong extragalactic magnetic field ~ 10 nG, to reduce the excessive anisotropy.

Subject headings: ISM: cosmic rays – ISM: magnetic fields – Galaxy: structure

1. Introduction

The origin of ultra-high-energy cosmic rays (UHECRs) is still unknown, despite intense theoretical studies and observational efforts. A new generation of detectors have collected, In the last decade, data with unprecedented statistics in both hemispheres. The Pierre Auger Observatory (Abraham et al. 2004) (hereafter Auger), operating in Argentina since 2004, is the largest observatory, with ~ 3000 km² effective detection area, and an integrated exposure of 66452 km² sr yr as of March 31st, 2014, mostly in the Southern sky. Telescope Array (Kaway et al. 2008) (hereafter TA), operating in Utah (USA) since 2007, covers ~ 700 km², and obtained an integrated exposure of 8600 km² sr yr as of May 11th, 2015, in the Northern sky.

The results reported by the two international collaborations (TA and Auger) concerning the energy spectrum, composition and angular distribution show some potentially significant differences. While a joint analysis working group concluded that the UHECR composition estimated by both experiments are compatible (Unger et al. 2015), the TA and Auger spectra appear to be different in shape, and an intermediate-scale anisotropy has been reported by the TA collaboration, while the Auger skymap does not show a statistically significant deviation from isotropy despite its larger exposure. While the difference in the spectra might possibly be due to energy-dependent systematics, we explore here the possibility that one or several source(s) in the Northern sky is (are) responsible for both the excess in the high-energy spectrum and to the so-called hotspot in the TA data.

Although the conjunction of these two observations may appear natural and consistent at first sight, with a particularly intense and/or nearby source producing a larger flux than average as well

¹Racah Institute of Physics, The Hebrew University of Jerusalem, 91904 Jerusalem, Israel

²Laboratoire Astroparticule et Cosmologie, Université Paris Diderot/CNRS, 10 rue A. Domon et L. Duquet, 75205 Paris Cedex 13, France

as a distinct cluster of events, the quantitative study of this conjunction rather points towards a severe conflict. As it turns out, and will be demonstrated in the present study, the excess in the TA flux compared to Auger is so large above ~ 50 EeV, that a much stronger anisotropy than the one observed is to be expected in general. While large deflections of the UHECRs by intervening magnetic fields may be invoked as a way to “wash out” the anisotropy, this seems essentially impossible if the flux is dominated by protons, and even in the case of heavier nuclei, large deflections tend to reduce the possibility of strong localised flux excesses, notably in the case of transient sources, because they spread the flux over larger time windows.

In order to quantify the problem at hand and to estimate the likeliness of such a combination of observations, we carry out detailed simulations of UHECR propagation in both the intergalactic medium (IGM) and the Galaxy, and distinguish between two general classes of sources: transients and steady. In the transient case, we use a specific model for the sources, based on GRBs (Globus et al. 2015), which reproduces both the spectrum and composition observed by Auger. Some characteristics of this model, such as the source composition and spectrum and the distribution of maximal energies and intrinsic luminosities among sources, are also kept as a reference for the steady source case. The first three are roughly essential for consistency with the Auger data. The last one is not, but lacking other information it is as good as any. Overall, we expect the results presented here to be generic and qualitatively independent of the specific nature of the sources.

We first investigate, in Sect. 2, the significance of the difference between the Auger and TA measurements. We then present in Sect. 3 a simple analytical estimate to determine the conditions under which a single source could contribute at a high level. In Sect. 4 we discuss the Monte Carlo simulations, where we take into account the propagation of the UHECRs from their sources to the Earth, including the model parameters and the procedure used to generate Auger-like and TA-like data sets from which sky maps can be built and analysed. We present, in Sect. 5, the results of our simulations, applying definite criteria to assess the similitude or compatibility of the simulated data

sets with the actual observational data. Finally, we summarise the results and discuss their possible implications in Sect. 6.

2. Are the UHECR northern sky and southern sky significantly different?

The possible difference in composition of the UHECRs observed by TA and by Auger has been widely discussed, after the claim by TA that their data is compatible with a pure proton composition (see for instance Tinyakov et al. (2015)), whereas Auger reports a gradual, but very significant trend towards higher mass nuclei around 10 EeV Aab et al. (2014a,b). The TA data is not inconsistent with the transition towards heavier elements inferred from the Auger data (Unger et al. 2015) (see however Shaham & Piran 2013, for a different interpretation of the data).

The difference in the clustering of events as well as in the energy spectrum appears more striking, and apparently more significant. While no significant small or intermediate-scale anisotropy can be observed in the Auger data (the largest departure from isotropy was found to have a post-trial probability of $\sim 1.4\%$ (Aab et al. 2015)), the TA Collaboration reported a so-called hotspot, with a 20° angular scale, near the constellation Ursa Major. The chance probability of observing such a clustering anywhere in the sky is $3.7 \cdot 10^{-4}$, equivalent to a one-sided probability of 3.4σ (Tinyakov et al. 2015). A second anisotropy analysis of the highest energy events (above 57 EeV) uses the two-point correlation function and compares the number of pairs of events separated by less than a given angular scale, to what is expected with the same exposure map for a purely isotropic flux. This test yields a minimal chance probability of $\sim 10^{-3}$ at angular scales between 20° and 30° (Tinyakov et al. 2015).

While such levels of significance are too low to be conclusive, it should be considered together with another difference, regarding the energy spectrum above ~ 50 EeV. Fig. 3 depicts the Auger and TA data, where a shift of -13% has been applied to the TA energy scale, as recommended by the Auger-TA joint working group (Unger et al. 2015). The TA spectrum clearly shows a significant excess at higher energy, at least if one considers only the statistical error bars (shown on

the plot). A systematic uncertainty with a rather strong energy dependence would be needed to explain such a difference.

After scaling down the energy by 13% there are 83 highest energy TA events above 50 EeV. They correspond to an exposure of $8600 \text{ km}^2 \text{ sr yr}$ (Matthews 2015). On the other hand, Auger reports 231 events above 52 EeV, for an exposure of $66452 \text{ km}^2 \text{ sr yr}$. Given the shape of the spectrum between 50 and 60 EeV, this extrapolates to ~ 290 events above 50 EeV. If the Auger flux is assumed to represent the average UHECR flux in the absence of anisotropy, then the expected number of events for TA is ~ 38 . The actual integrated flux of TA would thus need to be a 7σ upward fluctuation.

It thus appears unlikely that the UHECR fluxes observed by Auger and TA are just different realisations of an underlying roughly isotropic flux. Put together with the observation of the TA hotspot, the current data suggest the possibility that not only the apparent excess in the TA spectrum above 50 EeV is real (unless large energy-dependent systematic uncertainties impact the measurements), but also that this excess could be caused by the contribution of one (or more) localised sources, which would dominate mostly in the Northern sky. Quantitatively, if the integrated flux of Auger above 50 EeV represents an average contribution of typical sources distributed more or less isotropically over the sky, the corresponding contribution in the TA data should be $\sim 38 \pm 6$ events, which leaves $\sim 45 \pm 6$ for the putative additional source(s). In other words, if the difference between the two spectra is taken seriously and attributed to the contribution of a dominant source, this source may represent 45%–60% of the total Northern sky flux.

To this end, we do not limit ourselves to the consideration of the spectrum. A satisfying model must not only provide two different spectra in the Northern and Southern hemispheres, but also reproduce the anisotropy patterns: it must i) be compatible with isotropy in the Southern sky (i.e. not produce an anisotropy signal much stronger than the warm spot reported around the direction of Cen A, with a 1.4% post trial chance probability to arise as a fluctuation of an isotropic flux), and ii) provide a hotspot in the Northern sky with a typical angular scale of 20° .

Concerning the other observable of UHECR phenomenology, namely the composition, it is taken into account here in a generic way. In Globus et al. (2015), some of us have developed a model based on the acceleration of particles in the mildly relativistic internal shocks of gamma-ray bursts (GRBs). This model reproduces the spectrum and composition¹, both below and above the ankle (Globus, Allard, Parizot 2015). From a phenomenological point of view, the main features of this model are a low value of the maximum energy for protons at the sources, a hard source spectrum for all nuclei except protons (which have a significantly softer spectrum), and a source composition with a metallicity higher than the usual Galactic cosmic-ray component by a factor of ~ 10 . These are considered here as generic features of a "working model", providing a suitable description of the average UHECRs, independently of the actual sources, whether GRBs, other types of transient sources (like tidal disruptive events, see e.g. Komossa (2015)), or steady sources. For the purpose of the anisotropy analyses of this paper, the main relevant ingredient is the composition of the UHECRs with an energy larger than 50 EeV, which is thus assumed to be the same as that of our explicit GRB model (Globus et al. 2015), but without prejudice regarding the nature of the sources.

3. Analytical estimates

3.1. Transient vs permanent sources

We describe now a simplified analytical investigation of the conditions under which an individual source can be responsible for a significant fraction of the total UHECR flux observed on Earth above an energy E_{th} (e.g. $E_{\text{th}} = 50 \text{ EeV}$). In parallel, we estimate under the same conditions the angular size of this source in the sky.

As can be easily understood, the situation is different depending on the nature of the sources, whether transient or permanent. In both cases, the apparent angular size of a given source on the sky depends on the deflections of the particles by

¹in order to reproduce the observed UHECR flux we had to assume that cosmic-rays carry most of the energy dissipated at the internal shock especially in the case of low luminosity GRBs.

the intervening magnetic fields². However, the apparent flux level of a source cannot be estimated in the same way for transient and steady sources. Obviously, we can only see a transient source when it is active towards us, i.e. when the difference in time between the moment when we are observing it and the moment when it was actually active matches the particle propagation time. But the *spread* in this propagation time is what sets the instantaneous flux level. For a given total amount of energy emitted by the source, the apparent luminosity is simply inversely proportional to the spread of the time delays. In practice, we consider as a transient source a source for which the typical variation of the intrinsic luminosity timescale is shorter than the propagation time delay from the source to the Earth. In this case, the effective luminosity is dictated by the total energy release during the transient event divided by the propagation time spread. We also assume, for the sake of simplicity, that the sources are standard candles. This is a conservative assumption, since a spread in the intrinsic source luminosities typically increases the variance of the contribution of the dominant source to the total flux, so the probability to obtain a higher flux fraction becomes larger (Blaksley et al. 2013).

Three steps of propagation, associated with different types of deflections and time delays, can in principle be distinguished: i) around the source, before the freshly accelerated UHECRs reach the IGM, ii) in the IGM between the source and our Galaxy, and iii) in our Galaxy, up to Earth. For the analytical estimates below, we gather these contributions into one standardised step, corresponding to the propagation of particles through a homogeneous medium filled with an isotropic turbulent magnetic field with a coherence length $\lambda_c \equiv \lambda_{\text{Mpc}}$ Mpc and intensity $B_{\text{rms}} \equiv B_{\text{nG}}$ nG. This is of course a very crude assumption, but it gives an idea of the link between the deflections and the scale of the intervening magnetic fields. Note that the specific influence of the Galactic magnetic field (GMF) is analysed in more detail in the following sections, as it turns out to play an important role, especially in the case of transient sources.

²we don't consider here the possibility that the source is extended and the observed size reflects its intrinsic scale.

In the limit of the weak scattering regime, where the Larmor radius of the cosmic-ray is larger than the turbulence scale of the magnetic field, the typical scale of the angular deflections of a particle with charge Z and energy $E \equiv E_{20} \times 10^{20}$ eV, coming from a source at a distance $D_s \equiv D_{\text{Mpc}}$ Mpc, is given by (Waxman & Miralda-Escude 1996):

$$\Delta\theta \approx 0.36^\circ Z E_{20}^{-1} B_{\text{nG}} D_{\text{Mpc}}^{1/2} \lambda_{\text{Mpc}}^{1/2}. \quad (1)$$

If the dominant class of nuclei at 50 EeV is CNO (Globus, Allard, Parizot 2015), the angular deflection is of the order of 14–18° in a nanogauss EGMF with a Mpc coherence length for a source located at 10 Mpc, or 7.5–10° for a source located at 3 Mpc. In comparison, the typical deflection in a 5 μG GMF with a coherence length of 200 pc over 1 kpc, is of the same order, around 8–10°.

We now turn to the conditions under which a source may contribute a given fraction of the total UHECR flux received on Earth. In principle, this fraction depends on energy, as the apparent source spectrum is expected to be different from the overall UHECR spectrum shaped notably by the GZK horizon effect. We thus consider only the integrated flux above a given energy, E_{th} (e.g. $E_{\text{th}} = 50$ EeV), and denote by η_{flux} the fraction of the total flux above that energy, which is contributed by the individual source. In all cases, we assume that the source emits UHECRs isotropically.

Note that, in principle, an excess in the spectrum in some part of the sky could be due to the contribution of two sources located by chance in the same hemisphere, rather than to the contribution of just a single source. However, a simple reasoning shows that this is in general much less probable. Essentially, the flux from one source is typically reduced by a factor of 2 if its distance is increased by a factor of $\sqrt{2}$. Now, it appears that the chance probability for one source to contribute a substantial fraction of the UHECR flux is relatively low, of the order of a few percent in the favorable scenarios. This is related to the probability to find a source closer than some distance D , which we may write $\mathcal{P}_1(D)$. The probability to find two sources in the same hemisphere closer than the distance $\sqrt{2} \times D$, i.e. in a volume $2\sqrt{2}$ larger, is then given by $\mathcal{P}_2(\sqrt{2}D) \simeq \frac{1}{2}[\mathcal{P}_1(\sqrt{2}D)]^2 \simeq 4 \times \mathcal{P}_1(D)^2$. Since $\mathcal{P}_1(D)$ is much smaller than 1/4, this has a much smaller probab-

ity. Therefore, in the analytical exploration below, we consider only the case of one dominant source being responsible for the excess in the overall flux.

3.2. Transient sources

In the case of bursting sources, the apparent flux of a source, Φ_{app} , is governed by its total energy (emitted in the form of UHECRs above E_{th}), E_s , its distance, D_s , and the average time spread, Δt , over which it is visible from Earth in the considered energy range. It is given by:

$$\Phi_{\text{app}} = \frac{E_s}{4\pi D_s^2 \Delta t}. \quad (2)$$

This should be compared with the average UHECR flux on Earth above E_{th} , Φ_{UHECR} , which can be approximately expressed in terms of the average source energy, E_0 , the source rate, $R = R_{-9} \times 10^{-9} \text{ Mpc}^{-3} \text{ yr}^{-1}$, and the GZK horizon scale, $H = H_{100} \times 100 \text{ Mpc}$, as:

$$\Phi_{\text{UHECR}} \approx E_0 R H. \quad (3)$$

In the above-mentioned magnetic field configuration, the spread in the time delays is approximately given by (Waxman & Miralda-Escude 1996):

$$\Delta t \approx (30 \text{ yr}) Z^2 E_{20}^{-2} B_{nG}^2 D_{\text{Mpc}}^2 \lambda_{\text{Mpc}}. \quad (4)$$

Note that, here, we abusively use the expression for the average time delay of the particles, instead of its spread over an ensemble of particles. This is not strictly correct, and indeed in the detailed simulations discussed in the next sections, the flux level of the sources is determined by the actual propagation time of each individual particle, obtained through a full Monte-Carlo procedure, taking also into account the rigidity losses along the way. However, for the current analytical estimate, we keep the above formula which has the advantage of providing an explicit dependence in the various parameters. By this, we acknowledge the fact that, according to the simulations, the spread in the time delays of the bulk of the particles is indeed of the same order as the average time delay.

From Eqs. (2) and (11), we can simply write the ratio between the flux of the source under study and the total flux expected on average (over space

and time in the local universe, i.e. over the so-called *cosmic variance*) above E_{th} . This will be referred to below as the source-to-average-total (or STAT) flux ratio. It reads:

$$\begin{aligned} \eta_{\text{flux}} &\equiv \frac{\Phi_{\text{app}}}{\Phi_{\text{UHECR}}} = \frac{E_s}{E_0} \frac{1}{R \Delta t} \frac{1}{4\pi D_s^2 H} \\ &\approx 2.7 \cdot 10^4 \xi R_{-9}^{-1} E_{20}^2 Z^{-2} B_{nG}^{-2} D_{\text{Mpc}}^{-4} \lambda_{\text{Mpc}}^{-1} H_{100}^{-1} \end{aligned}$$

where we noted $\xi = E_s/E_0$ the over-luminosity of the source under consideration. In the case of standard candles, of course, $\xi = 1$.

Obviously, a very nearby source will give a very high flux fraction. However, η_{flux} depends very strongly on the source distance, as its fourth power, since D_s comes in both through the trivial $1/D_s^2$ flux factor, and through the apparent time spread of the source, proportional to D_s^2 . Therefore, one needs to estimate the probability to find a source within a given source distance.

The average number of transient sources, active at any given time, in a sphere of radius D_s , is $\langle N \rangle = R \times \Delta t \times \frac{4}{3}\pi D_s^3$. For low values of $\langle N \rangle$, this is also the probability to find a source within D_s . Note that we are implicitly interested in situations where this number is low indeed, since we are interested in the dominant source, whose flux compares to the total flux of all other sources contributing in that energy range. It must thus be exceptional by its proximity and/or small time spread, which would not be the case if $\langle N \rangle$ were close to 1 or more.

Equation (5) can now be inverted to give the distance at which a source with over luminosity ξ must be located to provide a given STAT ratio, η_{flux} :

$$D_s(\eta_{\text{flux}}) \simeq (12.8 \text{ Mpc}) \eta_{\text{flux}}^{-1/4} \xi^{1/4} E_{20}^{1/2} (Z B_{nG})^{-1/2} \cdot (R_{-9} \lambda_{\text{Mpc}} H_{100})^{-1/4}. \quad (6)$$

The corresponding probability, for $\xi = 1$, is then found to be:

$$\begin{aligned} \mathcal{P}(\eta_{\text{flux}}) &\simeq \langle N(D_s(\eta_{\text{flux}})) \rangle \\ &\simeq 4.3\% \eta_{\text{flux}}^{-5/4} E_{20}^{1/2} (Z B_{nG})^{-1/2} R_{-9}^{-1/4} \lambda_{\text{Mpc}}^{-1/4} H_{100}^{-5/4}. \end{aligned} \quad (7)$$

As an example, let us consider CNO nuclei at $E \simeq 50 \text{ EeV}$ and a source rate of one burst per Gpc^3 per year. If the deflexions and time delays

are similar to what would produce a homogeneous turbulent EGMF with $B_{\text{nG}} = \lambda_{\text{Mpc}} = 1$, the probability that a dominant source contributes at the same level as the rest of all other sources in one hemisphere, i.e. $\eta_{\text{flux}} \simeq 1/2$ is of the order of 3%. Although not common, this does not seem particularly unlikely. However, one must also consider the angular extension of such a source.

Using Eq. (1), one obtains the angular size expected for a source that would contribute a fraction η_{flux} of the global UHECR flux, i.e. be located at distance $D(\eta_{\text{flux}})$, given by Eq. (6):

$$\Delta\theta(\eta_{\text{flux}}) \simeq 1.3^\circ \eta_{\text{flux}}^{-1/8} \xi^{1/8} E_{20}^{-3/4} (ZB_{\text{nG}})^{3/4} \lambda_{\text{Mpc}}^{3/8} (R_{-9} H_{100})^{-1/8}. \quad (8)$$

As can be seen, the dependence on the various parameters is weak, except on the ratio E/ZB , which is simply the Larmor radius of the particles (times c/e). For CNO nuclei at 60 EeV in a nanogauss field, one obtains $\Delta\theta \simeq 7-9^\circ$. This appears too small to account for the TA observations. As a matter of fact, a source that would contribute, say, 50%, of the total flux and would span over 9° in the sky. Therefore, if the apparent difference in the UHECR spectrum between the northern and southern hemispheres is to be attributed to the contribution of one dominant source, then the angular spreading of the source must be due mostly to the action of the GMF, at least if the extragalactic magnetic field (EGMF) does not significantly exceeds a nanogauss. For a pervading EGMF of 3 nG, say, the angular size would increase by a factor 2.3, while the probability of a given contribution to the overall flux would decrease by a factor 1.7 (see Eq. (7)). Note that the angular size of a source could be increased if the source is surrounded by a large magnetic halo, which by itself has a large angular extension over the sky. However, in the case of transient sources, such a halo would also considerably extend the time spread of the UHECRs from that source, and thus strongly reduce its apparent luminosity.

A key question is thus whether the GMF can increase the angular spreading of a source sufficiently to reconcile the idea that the spectral differences between the two hemispheres are due to a dominant source with the anisotropy data. Unfortunately, the GMF is not known with enough precision to give a definite answer to this question.

We discuss this point below in more detail, in particular with the comparison between the situations in the northern and southern hemispheres, which turn out to be different, but we recall here the estimate of Sect. 3.1, which gave $\sim 8-10^\circ$ for a length of 1 kpc through a $5 \mu\text{G}$ with $\lambda_c = 200 \text{ pc}$. Obviously, the deflections depend on the length of the trajectory through the GMF, and thus on the direction of the source, within or away from the Galactic disk. In addition, the size of the magnetic halo above the disk appears to be a crucial parameter (as well as its coherence length). An extension much larger than 1 kpc, still with significant magnetic field, would lead to significantly larger deflections, and could explain the absence of a well marked, small scale anisotropy, even if a large fraction of the total flux can be attributed to one source with relatively limited angular spread at the entrance of the Galaxy.

Finally, it is instructive to calculate the typical time spread of the UHECRs detected from a dominant source with STAT ratio η_{flux} . This is easily obtained as a function of the various parameters, by reporting the required source distance, $D_s(\eta_{\text{flux}})$, given by Eq. (6), into the expression of Δt in Eq. (4). One finds:

$$\Delta t(\eta_{\text{flux}}) \simeq (4.9 \text{ kyr}) \times \eta_{\text{flux}}^{-1/2} \xi^{1/2} Z E_{20}^{-1} B_{\text{nG}} \lambda_{\text{Mpc}}^{1/2} H_{100}^{-1/2}. \quad (9)$$

For CNO at 60 EeV, the typical time spread is thus of the order of a few tens of kiloyears for the dominant source. It can be seen that a larger EGMF allows for a larger time spread, but only linearly, whereas Δt increases as the square of the magnetic field for a given source distance. Thus, the larger value of Δt allowed for a larger magnetic field is actually related to the necessity of having a closer source, which then reduces the probability of such an occurrence (see Eq. 7).

3.3. Steady sources

We now turn to the case of steady sources, which inject UHECRs in the intergalactic medium at a constant luminosity, L_0 . Like before, we allow for a different luminosity of the source under consideration, L_s , and note $\xi \equiv L_s/L_0$. The flux received from that source is simply:

$$\Phi_{\text{app}} = \frac{L_s}{4\pi D_s^2}, \quad (10)$$

while the average UHECR flux from all sources within the GZK horizon, H , is:

$$\Phi_{\text{UHECR}} \approx L_0 n_s H, \quad (11)$$

where $n_s \equiv n_{-5} 10^{-5} \text{ Mpc}^{-3}$ is the source density.

The STAT flux ratio is thus given by:

$$\eta_{\text{flux}} = \frac{\xi}{4\pi D_s^2 H n_s} \simeq 80 \xi D_{\text{Mpc}}^{-2} H_{100}^{-1} n_{-5}^{-1}. \quad (12)$$

The distance where a source must be to account for a flux ratio η_{flux} is thus:

$$D(\eta_{\text{flux}}) = (8.9 \text{ Mpc}) \eta_{\text{flux}}^{-1/2} \xi^{1/2} n_{-5}^{-1/2} H_{100}^{-1/2}. \quad (13)$$

As in the case of transient sources, the probability to find a source within this distance is essentially the average number of sources in the corresponding volume, namely $\langle N \rangle = \frac{4}{3}\pi D_s^3 \times n_s$. This gives:

$$\mathcal{P}(\eta_{\text{flux}}) \simeq 3.0\% \xi^{3/2} \eta_{\text{flux}}^{-3/2} n_{-5}^{-1/2} H_{100}^{-3/2}. \quad (14)$$

Regarding the angular spread of such a source, it is estimated as before using Eq. (1):

$$\Delta\theta(\eta_{\text{flux}}) \simeq 1.1^\circ \eta_{\text{flux}}^{-1/4} \xi^{1/4} Z E_{20}^{-1} B_{\text{nG}} \lambda_{\text{Mpc}}^{1/2} n_{-5}^{-1/4} H_{100}^{-3/4}. \quad (15)$$

The dependence on the various parameters is larger than in the case of transient sources, because the flux level does not depend on any time spread, and thus on the magnetic field. However, the source angular extension does not depend strongly on the source density, which has a greater influence on the probability of the situation under investigation. For CNO nuclei at 60 EeV in a nanogauss magnetic field, we obtain an angular size of the order of $10\text{--}15^\circ$, which is again too low to account for the TA hotspot. However, a stronger magnetic field can increase this angular size linearly, and a contribution of the GMF may also be important. Note that in a case of a pure proton composition scenario, the angular size of a hotspot would be smaller than $\sim 3^\circ$ for a nanogauss magnetic field and a source distance of 10 Mpc. Thus it would be even more difficult to account for the anisotropy observed by TA.

4. Model and simulations

In the previous section, we estimated the conditions under which one source may contribute a significant fraction of the total UHECR flux, and the

probability that this situation occurs at a given moment in time, in a given location of the universe. The main outcome is that this probability may be of the order of a few percent for a relatively wide range of parameters, in the case of steady sources as well as in the case of transient sources. Concerning the angular size of this source on the sky, it appears that the EGMF alone is usually too low to spread the particles over a region much larger than $10\text{--}15^\circ$ (CNO nuclei at 60 EeV), so that such a source would produce significant small-scale anisotropies, at variance with the current observations. However, larger values of the EGMF in the direction of the source or a significant contribution of the GMF to the overall deflections could in principle allow the scenario under study to be viable.

In this section and the next, we use a complete Monte Carlo simulation of the source distribution and history and of the UHECR propagation to study the transient and permanent source scenarios in more detail, taking into account the GMF and the actual exposure of Auger and TA in their respective part of the sky, and comparing our simulated sky maps and spectra with the data. The criteria used to assess the overall compatibility of these sky maps with the actual data are presented in Sect. 5. Here, we describe the central numerical tool of the simulation, based on our Monte-Carlo propagation code, which is used to compute the propagation of UHECRs from individual point-like sources, taking into account their energy losses, their nuclear transmutation through the interaction with the cosmological photon background, and their deflections in the intervening magnetic fields (see Allard et al. 2005; Globus, Allard, Parizot 2008, for more details about our propagation code).

4.1. General ingredients of the simulations

4.1.1. Galactic and extragalactic magnetic fields

Concerning the magnetic deflections and the distribution of UHECRs over the sky, we first follow the trajectory of individual particles through the EGMF, assuming a random Kolmogorov-like turbulent field with r.m.s. value B_{EG} , and a principal turbulent scale of 1 Mpc (which corresponds to a coherence length $\lambda_c \simeq 0.2 \text{ Mpc}$). To model the EGMF, we follow the numerical procedure of

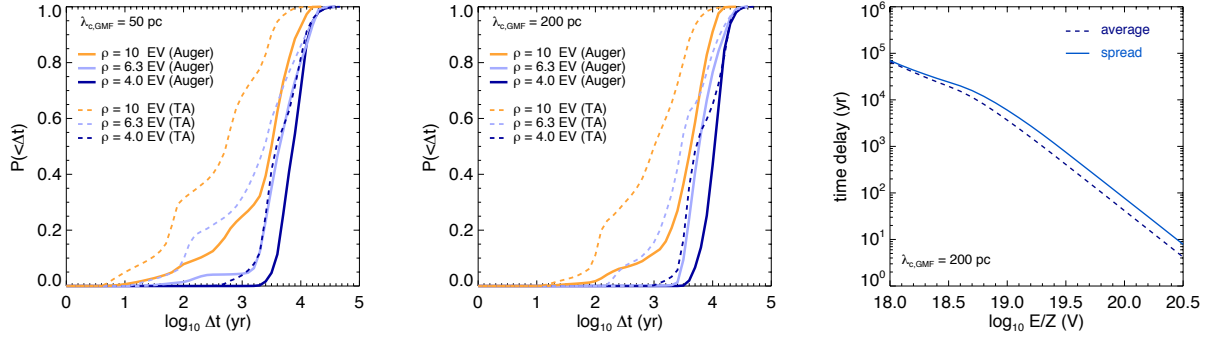


Fig. 1.— Left and middle: cumulative distributions of the spread in time delays due to the GMF in the TA sky (dashed lines) and in the Auger sky (solid lines) for different values of the rigidity, for $\lambda_{c,GMF} = 50$ pc (left) and for $\lambda_{c,GMF} = 200$ pc (middle). The ordinate shows the probability that the time delay is shorter than the value in abscissa. Note that the TA time delays are significantly shorter. Right panel: average over all (incoming or outgoing) directions of the time delays and their spread due to the GMF, as a function of the rigidity of the particles. At high rigidities, they both scale as $\Delta t \propto (E/Z)^{-2}$, as expected in the weak scattering regime (see Eq. 4).

Giagalone & Jokipii (1999). The EGMF is assumed to be distributed homogeneously throughout the universe. Although this is admittedly not realistic, it allows us to explore the influence of the magnetic field, with a wide range of possibilities, from 0.01 nG, below which the effect would be essentially negligible on the present studies, to 10 nG, which may be considered as a maximum value for a consistent and pervasive magnetic field. As can be noted from the analytical study of Sect. 3, the magnetic field value and coherence length always appear through the product $B_{EG} \times \lambda_c^{1/2} = (1 \text{ nG Mpc}^{1/2}) B_{nG} \lambda_{Mpc}^{1/2}$. Therefore, for the present study, it is not necessary to vary these two parameters separately. We thus chose to keep the coherence length fixed, and simply vary B_{EG} , in the range from 0.01 nG to 10 nG. For instance, the case corresponding to $B_{EG} = 10$ nG and the default value of $\lambda_c = 0.2$ Mpc is equivalent to a case with $B_{EG} \sim 4.5$ nG and $\lambda_c = 1$ Mpc.

We then take into account the propagation in the Galaxy. The large-scale structure of the GMF is modeled as in Jansson & Farrar (2012) (hereafter JF12). In the following description we use cartesian (x, y, z) and cylindrical coordinates (r, ϕ, z) . The Galactic center is at the origin, Galactic north is in the positive z -direction, and the Sun is located at $x = -8.5$ kpc. In the JF12 model,

the magnetic field is set to zero for $r > 20$ kpc and in a 1 kpc radius sphere centered on the Galactic center. The large-scale coherent field, hereafter denoted by B_{reg} , involves three separate components: a disk field, a halo field, and an out-of-plane halo component, the latter being motivated by radio observations of external galaxies (Krause 2007; Beck 2009). The GMF disk component is divided into eight logarithmic spiral regions and its strength varies from ~ 0.1 to $4 \mu\text{G}$. Two large-scale reversals occurs between spiral arms 2 and 3, and 6 and 7. The vertical extension of the disk field is 0.4 kpc above the disk midplane. The GMF halo component is a purely toroidal field with an exponential scale height, $B_\phi \sim B_0 \exp(-|z|/z_0)$ ($z_0 \sim 5$ kpc), and with spatial extensions and amplitudes that are different in the north and the south. In the north, $B_0 = 1.4 \mu\text{G}$, while in the south $B_0 = -1.1 \mu\text{G}$. The change of sign of the toroidal field implies the existence of a current sheet at the equator. In the northern halo, the field extends to $r \sim 9$ kpc, while the southern component stretches to $r \sim 16$ kpc, as can be seen in Figure 5 of JF12. The third component of the GMF regular field is the out-of-plane halo component, which is axisymmetric and purely poloidal and reaches its maximum value, $\sim 3 \mu\text{G}$, at the Galactic center (Figure 6 of JF12). To the regular

coherent field described above, we add a purely turbulent component, B_{turb} , following the numerical procedure of Giacalone & Jokipii (1999). We assume a Kolmogorov-like spectrum and a coherence length $\lambda_{\text{c,GMF}}$ of either 50 pc or 200 pc. The r.m.s. value follows the magnitude of the regular component with an overall enhancement factor of 3. Finally, we also include a so-called striated magnetic field, which consists of an anisotropic turbulent component, B_{str} , whose orientation is aligned with the large scale coherent field, but whose strength and sign vary on a small scale. Following JF12, we use $B_{\text{str}}^2 = 1.4 B_{\text{reg}}^2$. This assumes that the striated field is generated from the regular field by shear. Another possible origin of the striation could be the compression of the isotropic turbulence (Beck, private communication). However for the present study we follow the prescription of JF12. The coherence length of the striated field is assumed to be 100 pc. The total GMF used in our calculations is thus $B_{\text{GMF}} = B_{\text{reg}} + B_{\text{str}} + B_{\text{turb}}$. The resulting local value of the GMF (near the Earth) is consistent with the 6 μG value inferred from observations (Beck 2008).

We also consider the possible presence of a magnetic field around the source itself. In the absence of a well defined model, we simply assume here that the sources are embedded in a magnetic field similar to that of our own Galaxy.

4.1.2. Effect of the Galactic magnetic field

The GMF becomes important when the EGMF is typically smaller than ~ 0.3 nG. In these cases its contribution is significant and may even dominate the deflection and the corresponding time delays, as far as the closest sources are concerned. We recall that the typical deflection of particles at rigidities 8-9 EV is smaller than 10° in the extragalactic nanogauss field for a source located at 10 Mpc (see Eq. 8). At these rigidities the deflections by the GMF are of the order of 10° to 20° , depending on the arrival direction of the particle, as explained below.

The GMF has several important effects. First, of course, it deflects the particles and makes a given source appear larger on the sky. This effect adds to the deflections through the EGMF. Second, it may cause some magnification or demagnification of the sources, depending on the arrival direction of the particles in the Galaxy (see

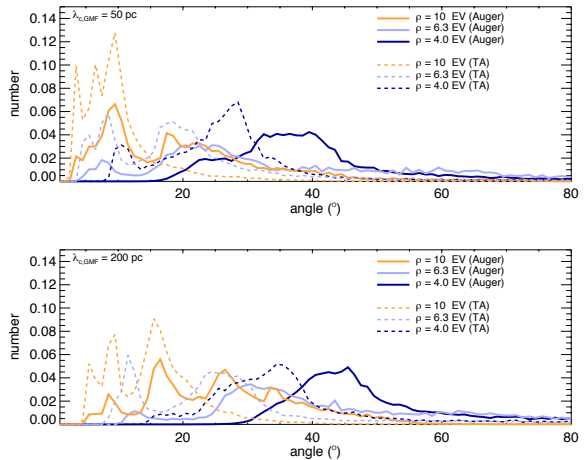


Fig. 2.— Normalised histograms of the angular spreads of the sources visible in the TA sky (dashed lines) and in the Auger sky (solid lines), for different values of the rigidity. Top panel: $\lambda_{\text{c,GMF}} = 50$ pc; bottom panel: $\lambda_{\text{c,GMF}} = 200$ pc. The ordinate shows the probability that a given source be located in a direction of the sky for which the variance of the angular shift between the position of the source and the actual arrival direction of an observed UHECR from that source is equal to the value in abscissa.

for instance Harari, Mollerach, Roulet (1999)). Indeed, a small solid angle around some specific directions in the sky (as observed “backwards” from the Earth) may gather the particles coming from a larger (respectively smaller) solid angle at the entrance of the Galaxy, so that the sources located in these directions can appear with a larger (resp. smaller) flux than if no deflections applied. Like all effects related to the magnetic field, this effect depends on the rigidity of the particles, i.e. it may select a given mass range at a given energy, or a given energy range for a given type of nuclei. This effect was discussed in Rouillé d’Orfeuil et al. (2014), where magnification maps were also shown, so we do not discuss it further here. However, we recall that our simulations take it into account in a consistent way, by applying the relevant magnification factor to the flux of each individual source in the sky, depending on the arrival direction of their UHECRs.

The third effect of the GMF is that it intro-

duces some time delay, in addition to that caused by the EGMF. This effect is very important in the case of transient sources, since the spread in the time delays has a direct incidence on the apparent flux of a given source (see Sect. 3). Now, it is very interesting to note that the Northern and Southern hemispheres are not equivalent in this respect, due to the asymmetry of the GMF, notably the different northern and southern extensions of the Galactic halo. Smaller dispersions in the time delays are significantly more common in the part of the sky observed by TA than in the part of the sky observed by Auger. This result was obtained from a systematic study, where we divided the sky in 49152 pixels covering identical solid angles, and determined the variance of the time delays caused by the GMF for a large number of particles (256 on average, depending on the magnification) observed in the corresponding directions.

In Fig. 1, we show the cumulative distribution of the spread in time delays, assuming a random source position with equal probability in any direction of the sky. This probability is shown by the solid line curves in the case of UHECRs observed by Auger, while it is shown by the dashed line curves in the case of TA. We show the results for three different values of the rigidity, namely 10^{19} V, $10^{18.8}$ V and $10^{18.6}$ V. The first one corresponds for instance to C nuclei at 60 EeV (or O nuclei at 80 EeV or protons at 10^{19} eV), while the last one corresponds to Fe nuclei at 100 EeV. Fig. 1 clearly shows that the probability of a short time delay, is much larger if the source is mostly seen in the TA sky. Of course, this difference in the “northern” and “southern” time spreads introduced by the GMF is only relevant when the values are larger than the time spreads introduced by the EGMF. We find that this is essentially the case for EGMF values smaller than 0.3 nG, which is consistent with the EGMF-induced time delay estimated for the dominant source in Eq. (9). The average value of the time delays in the GMF and their spread over all possible directions is shown in the right panel of Fig. 1 as a function of the rigidity of the particle. At high rigidities, they both scale as $\Delta t \propto (E/Z)^{-2}$, as expected in the weak scattering regime (see Eq. 4).

The structure of the GMF introduces a similar difference regarding the angular spread of the sources, as shown in Fig. 2. The plots show the

variance of the particle deflections in the same conditions, i.e. for particles observed in the TA sky (dashed lines) and in the Auger sky (solid lines), for three values of the rigidity and two values of the field coherence length. The most probable angular spreads are typically smaller in the TA sky than in the Auger sky.

Finally, while a small spread in the UHECR time delays translates into a high instantaneous flux in the case of transient sources, it should be noted that additional time delays are likely to originate from the magnetic field in the environment of the source itself, which could be that of the host galaxy or extend from the scale of a local circumstellar environment up to the scale of a galaxy cluster (see the discussion in Takami & Murase (2012)). In our simulations, we simply assume that the typical time delays associated with the exit of the UHECRs from their sources to the general intergalactic medium is similar to those introduced by our own galaxies. Since the orientation of the host galaxy with respect to the line of sight (and to a possible source axis, in the case of beamed ejection of UHECRs) is a priori random, we draw randomly in the distribution of time spreads among different directions across the host galaxy.

4.1.3. General source properties

To build simulated sky maps corresponding to a given astrophysical scenario, we first need to choose the location of the sources. In the case of steady sources, we simply draw randomly the source locations in 3D space according to the source density, with equal probability in all directions of the sky. Although matter is not distributed uniformly in the local universe, this simplification has no significant incidence on our results, which are analysed from the point of view of their total energy spectrum and their intrinsic anisotropy, at intermediate angular scales, rather than their correlation with specific classes of sources or matter distribution. Note that the source density specified in each case is actually a comoving density (i.e. with a fixed average source number per comoving volume) and that we also allow for a possible evolution of the individual source power as a function of redshift. This, however, has no significant impact on the spectra and anisotropy patterns in the GZK energy range,

given the short horizon scale. In the case of transient sources, we also need to specify the time of their occurrence, which is chosen randomly according to a certain rate.

For definiteness, we choose the gamma-ray burst (GRB) source model described in Globus et al. (2015), where the UHECRs are accelerated at the internal shocks of GRBs, as a reference model. From this model, we borrow some characteristics, which may be considered as generic properties that typical source models must have to reproduce the Auger data, such as a mixed composition with high metallicity and a hard spectrum with low proton maximum energy. The same is assumed here for all sources, whether transient or steady.

Many properties may in principle vary from one class of sources to the other, none of which can however be directly inferred from the current data. For instance, while the average injection rate density, expressed in $\text{erg}^{-1}\text{Mpc}^{-3}\text{yr}^{-1}$, is well constrained by the observed flux, we do not know the total energy injected in the form of UHECRs by individual sources, nor even its average, which is directly related to the source density in the case of steady sources, or to the source occurrence rate in the case of transient sources. Until the sources are identified, these can essentially be regarded as free parameters in the general modelling of the UHECRs. In addition, it should be kept in mind that all sources may not have the same luminosity. In the absence of better-motivated assumptions, we adopt the relative luminosity distribution that results from the calculations in the framework of our GRB source model, and apply it throughout this paper. This is thought to be more realistic than the standard candle assumption. The corresponding transient source occurrence rate is $1.3 \cdot 10^{-9} \text{Mpc}^{-3}\text{yr}^{-1}$ (Wanderman & Piran 2010). We also explored 10 times larger and 10 times smaller rates, but found that it did not change the outcome of the study significantly (in conformity with the analytical estimates, where the rate appears with a power 1/8 as far as the apparent angular size is concerned, and 1/4 regarding the flux excess probability, see Eqs. 7 and 8).

Note that we consider sources emitting UHECR isotropically. This includes the case of transient sources although there are observational evidence and energetic arguments favoring a beamed emis-

sion from GRBs (Frail et al. 2001). While the assumption of an isotropic assumption has essentially no impact on our results for values of the EGMF of $\lesssim 1 \text{ nG}$ (at least as long as the contributions of the strongest sources are concerned), this is no longer true for larger values of the EGMF. Moreover, in the case of a beamed emission of UHECRs, the flux received from a given GRB event could also be affected by the angular spreading of the jet in the immediate vicinity of the source depending on the magnetic environment of the host galaxy and on the exact value of the beaming angle. Ignoring these potential complications, the predictions we make especially regarding the probability of a strong flux excess in the TA have to be considered as relatively optimistic, all the more when the assumed EGMF is of 1 nG or larger. Even in the framework of our simplifying hypotheses we will see however that it is extremely difficult to account for the present observational data with a transient source scenario.

4.2. Simulation procedure and analysis

4.2.1. Production of the simulated data sets

Once all the relevant parameters have been defined, we build the sky maps by picking individual UHECR events, one after the other, until we reach the required number to match the integrated flux seen by Auger above a reference energy of 5 EeV , namely 59500 events (as of March 31, 2014, for a total exposure of $66452 \text{ km}^2 \text{ sr yr}$). Although chosen arbitrarily, this energy is low enough for the UHECR flux to be considered essentially isotropic at this energy, and the corresponding number of events is large enough to not suffer from significant statistical fluctuation (including cosmic variance) in the Auger data.

The way we draw the individual events reflects the complexity of the underlying phenomenology. In the case of transient source, we first calculate numerically the all-particle spectrum for a given realisation of the GRB history in the universe, taking into account galactic and extragalactic time delay distributions. This calculation allows us to build probability tables for the energy distribution, the redshift distribution at a given energy, the discrete sources contribution at a given redshift and a given energy and for the different sources contributing significantly the probability

distribution of the different species and the associated distributions of deflexion angles. Our datasets are then produced by sampling successively these probability tables. We first draw the energy E of the particle, then we draw the redshift at which the particle was injected by its source in the intergalactic medium. Given the redshift, we then pick up an actual source, choosing randomly among the possible ones, in case there are several in the corresponding redshift range for the specific realisation of the distribution of sources under study. We then draw randomly the mass and charge of the particle. From there, we pick the deflection angle in the EGMF for a particle with the identified energy and charge coming from this particular source. Given the position of the source, we then know the arrival direction of the particle in the Galaxy.

At this stage, the study of Galactic deflections comes in. By inverting the result of a massive backwards propagation calculation (see the description of the method in Rouillé d'Orfeuil et al. (2014)), we obtained for each arrival direction outside the Galaxy the probability of being seen on Earth from a given direction in the sky. We can thus draw an actual arrival direction accordingly.

The final steps consist in two acceptance/rejection draws, to take into account the magnification factor (we draw a random number between zero and the maximum magnification factor at the relevant rigidity over the whole sky) and the exposure of the experiment under consider (Auger, TA, or a hypothetical full-sky, uniform exposure experiment). If the event is kept in these last steps, we attribute a reconstructed energy by applying a random Gaussian relative error to each event with a width of 15% in the case of Auger, and of 20% in the case of TA. The event is then included in the dataset and the procedure is repeated until the number of events with reconstructed energies above 5 EeV is 59500 in the case of Auger. This gives in average ~ 7700 events above 5 EeV in the case of TA as expected from the ratios of the time integrated exposures of the two observatories. The full dataset is used to calculate the observed spectrum while the 231 (respectively 83) highest energy events are selected in the Auger (respectively TA) sky to compare their intrinsic anisotropy to that of the observational data.

In the case of steady sources, the procedure

is exactly the same, except for the random draw of the redshift of the source, since the individual sources are assumed to be permanent and their contribution to the present flux is integrated over redshifts (i.e. look-back times).

4.2.2. *Exploration of the cosmic variance, statistical fluctuations and systematic differences*

Given the assumptions summarised above, the free parameters of the models are the EGMF value, the GMF coherence length and the source density or occurrence rate. For each set of these parameters, the observed spectra and the distribution of the UHECR events over the sky may be very different, depending on the actual position of the sources, and their occurrence time in the case of transient sources. The range of these variations is usually referred to as the cosmic variance. In order to explore these various possibilities, the procedure is repeated several times for each choice of the model parameters. Specifically, for each model we produce 1200 random realisations of the GRB explosion history, and 600 random realisations of the the source distribution in the universe in the case of steady sources. Then, for each of these realisations, we produce 10 random data sets with the intended statistics (i.e. 59500 events above 5 EeV in the Auger sky), whose differences reflect statistical fluctuations of the same underlying sky map, energy spectrum and composition. Thus, in total, we obtain 12000 and 6000 realisations of each individual astrophysical scenario.

4.2.3. *Anisotropy analysis*

Once generated, the data sets are analysed from the point of view of their intrinsic anisotropy, in order to assess their degree of compatibility with the actual data. For this, we use two standard analyses, which have been applied by the TA and Auger collaborations to their own data. The first one is the so-called 2-point correlation function analysis. It consists in computing the number of pairs of events with an angular separation smaller than a given angle θ , and compare this number to the numbers of pairs obtained from random data sets with the same total number of events, but built from a purely isotropy flux. One determines, for each angular scale θ , the fraction of isotropic data sets which have a larger number

of pairs within that angular separation than the data set under study. This can be noted $\mathcal{P}_{\text{iso}}(\theta)$, as it gives the probability that a purely isotropic UHECR flux would produce at least as many pairs of events separated by an angle lower than θ . In the following, we concentrate on the smallest value of $\mathcal{P}_{\text{iso}}(\theta)$, as θ varies from 1° to 45° , which we note \mathcal{P}_{min} . The corresponding angular scale is noted θ_{min} .

The second analysis of the anisotropy of the simulated data sets is a simple clustering analysis. It follows closely the analysis performed by the TA collaboration, which led to the identification of their so-called hotspot ???. For each simulated data set, we apply a circular “top hat” with an angular size of 20° around a given position in the sky, and simply count the number of events detected within that angular distance. We then compare this number with the number of events expected from a purely isotropic flux (with the same coverage map and exposure), and determine the significance of the corresponding clustering signal using the standard Li-Ma statistics (Li & Ma 1983). This significance of course depends on the position of the center of the circle in the sky map. After scanning the entire sky, we record the largest significance value obtained for the data set under consideration, and call it the raw (or unpenalised) hotspot significance. This value, which we note here σ_{hotspot} , is then compared with the corresponding value in the actual TA dataset.

5. Results

5.1. Comparing the simulated data sets with the actual Auger and TA data

In order to determine whether a given astrophysical scenario can account for the main features of the UHECR flux measured on Earth, we generate a large number of simulated data sets as described in the previous section, corresponding to the Auger and TA coverage maps and exposures, respectively, and then study the compatibility of these simulated data sets with the actual data. For this, we use general criteria based on the corresponding energy spectrum and the analysis of the intrinsic anisotropy of the data sets. The latter analysis is performed on sky maps which are built, for each realisation, with the same number of events as the data to which it is compared (i.e.

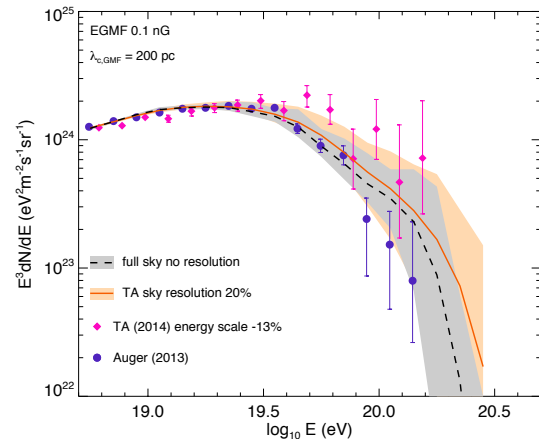


Fig. 3.— Propagated spectra for the GRB source model with $B_{\text{EGMF}} = 0.1$ nG. The dashed line shows the “infinite statistics” all-sky spectrum, averaged over 300 realisations of the astrophysical scenario. The gray area shows the range corresponding to the 90% cosmic variance (see text). The orange area corresponds to the spectra of 90% of the 3000 TA-like simulated data sets (10 per realisation), while the orange solid line is the average of these spectra over all 3000 data sets. The Auger and TA data are also shown, with $1\text{-}\sigma$ statistical error bars. The energy scale of the TA data set has been shifted down by 13% (see Unger et al. 2015).

with the 83 highest energy events in the case of the TA, and with the 231 highest energy events in the case of Auger).

5.1.1. Propagated energy spectrum

The first general result of the simulations is the propagated spectrum. An example is shown in Fig. 3 for a transient source scenario based on our GRB model with an EGMF r.m.s. value of 0.1 nG. The black dashed line shows the average spectrum over 3000 realisations of the same scenario (see Sect. 4.2.2). More precisely, the value in each energy bin is the average of the bin content for all the realisations. Note that the bin values for each realisation are not independent, as some realisations may involve for instance a particularly nearby and bright source, therefore leading to a flux that is consistently higher than average over many con-

secutive bins. The grey shaded area corresponds to the 90% fluctuation range of the individual bin contents.

The underlying astrophysical model is already known to reproduce the main features of the Auger UHECR data (Globus et al. 2015). Therefore, it is not a surprise that the spectrum shown in Fig. 3 is compatible with the Auger data, shown with the violet points on the plot. The TA data are also displayed, with a shift of -13% in the energy scale, to match the Auger spectrum at low energy.

The solid red line on Fig. 3 shows the average spectrum expected for the same model, assuming the TA exposure map (and an energy resolution of 20%). As can be seen, this average spectrum is higher than the average all-sky spectrum. More interestingly, the range of variations of the spectrum in this part of sky and with the TA statistics is found to be quite large. This is represented by the orange shaded area, which shows the 90% variation range (including both cosmic variation and statistical fluctuations). The top of this area appears to be still slightly below the TA data, which indicates that a UHECR flux as high as that measured by TA might be expected is at most a few percent of the cases, in the same scenario which otherwise gives an average spectrum similar to that of Auger.

5.1.2. Flux criteria

Among the large number of simulated data sets, we are interested in the specific realisations which produce a spectrum compatible with both with TA and Auger spectra (see an example in Appendix 6). Now, of course, we need to quantify the likeliness of such realisations. In order to perform a systematic analysis of the spectra associated with all the produced data sets, we establish a criterion of compatibility with the TA data by comparing the integrated fluxes above 50 EeV. We define N_{50} as the number of events above that energy. In the TA data set used in the present paper, which is obtained with a total exposure of $8600 \text{ km}^2 \text{ sr yr}$, there are 83 events with an energy larger than 57 EeV, which corresponds, after the above-mentioned downward shift of the energy scale, to $\simeq 50$ EeV. Therefore, the value of reference for TA is $N_{50} = 83$. In our simulated data sets, we allow for an upward or downward statistical fluctuation of this number by 1.5σ , i.e. we

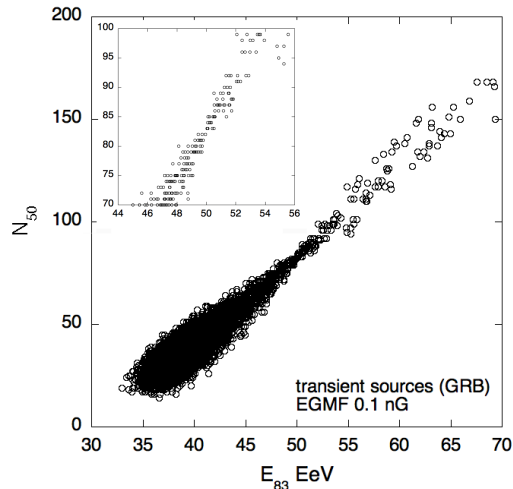


Fig. 4.— Correlation between the number of events above 50 EeV, N_{50} , and the energy of the 83rd most energetic event, E_{83} , in the TA-like simulated data sets, for the GRB transient source model with $B_{\text{EGMF}} = 0.1 \text{ nG}$.

set as a criterion that the TA-like simulated data sets must have a value of N_{50} between 70 and 97, in order to be judged compatible with the data.

Alternatively, after ordering the UHECRs in the simulated TA-like data sets by decreasing energies, we may ask what is the energy of the 83rd event, which we note E_{83} . Obviously, $E_{83} \simeq 50$ EeV in the actual TA data set. We can then use the value of E_{83} in the simulated data sets as another criterion to determine whether they may be compatible with the TA data, as far as the global spectrum is concerned. Of course, both values, N_{50} and E_{83} , are strongly correlated: the higher the energy flux, the larger the energy of the 83rd event. This is illustrated in Fig. 4. From this correlation plot, built with all 12000 simulated data sets, one can see that the criterion that $70 \leq N_{50} \leq 97$ is roughly equivalent to $47 \leq E_{83}(\text{EeV}) \leq 53$. This alternative criterion has a slight practical advantage in our analyses, because the sky maps we build always have the same number of events in the TA sky, namely 83, to allow for a direct quantitative comparison of their anisotropy patterns with those of the TA data, as discussed below.

A selection criterion should also be applied to the Auger-like simulated data set, notably to reject realisations for which the flux excess in the TA sky is due to a dominant source, which also contributes significantly to the UHECR flux in the Auger sky, thereby producing a spectrum that does not match the Auger spectrum at high energy. Since our Auger-like sky maps are built with 231 events, we use the value of the energy of the 231st event, E_{231} , to build a selection criterion. While $E_{231} = 52$ EeV in the Auger data, we accept all realisations for which $E_{231} \leq 57$ EeV. We found that this criterion is rejecting only a small fraction of the simulated data sets, which is due to the fact that the Auger data are generally well reproduced by our models.

5.1.3. Anisotropy criteria

The second challenging feature of the available data sets is their level of anisotropy. As it appears, the anisotropy level of the TA data is surprisingly low, when put into perspective with the observed flux excess. The general qualitative statement saying that a dominant source that would be responsible for that flux excess is likely to produce a strong anisotropy is indeed supported by our quantitative study, and it appears extremely challenging to reconcile both features of the data, as we show below.

Concerning the anisotropy, we use two complementary criteria. The first one is based on the two-point correlation function of the UHECR arrival directions. As indicated in Sect. 4.2.3, for each data set we compare the number of pairs of events with angular separation smaller than a given angle θ with the number of pairs expected in the case of a purely isotropy flux, for $1 \leq \theta(^{\circ}) \leq 45$. The largest departure from the isotropic expectations among the various angular scales is noted \mathcal{P}_{\min} . In the actual TA data set, the value of $\mathcal{P}_{\min} \simeq 10^{-3}$, which is reached at the angular scale of 22° . As shown below, most of the simulated data sets having a spectrum compatible with that of TA show a much larger \mathcal{P}_{\min} . We set a criterion requiring \mathcal{P}_{\min} to be between 10^{-5} and 10^{-2} , and that the angular scale at which \mathcal{P}_{\min} is reached has to be larger than 15° .

The second criterion is associated with the hotspot analysis, as described in Sect. 4.2.3. Using a top hat with an angular scale of 20° , the TA hotspot a Li-Ma significance of 5.1σ (Tinyakov et

al. 2015). We set as a criterion that the most significant departure from isotropy in the form of a hotspot should have a Li-Ma significance σ_{hotspot} between 4.6 and 5.6.

Finally, we apply an additional criterion to the Auger-like simulated data sets, requiring that the 231 highest energy events in the Auger sky do not show a much stronger anisotropy than the actual Auger data through the two-point correlation function analysis. We use again \mathcal{P}_{\min} as the relevant quantity, and reject all realisations for which 7 or more of the 10 data sets built from a given realisation have a \mathcal{P}_{\min} value smaller than 10^{-3} .

In the following subsections, we show the results of our simulations, confronting the data sets with the above flux and anisotropy criteria, first taken separately, and then taken together. Table 1 summarises them.

TA flux	$70 \leq N_{50} \leq 97$
TA flux	$47 \text{ EeV} \leq E_{83} \leq 53 \text{ EeV}$
TA 2-point	$10^{-5} \leq \mathcal{P}_{\min} \leq 10^{-2}$
TA 2-point	angular scale of $\mathcal{P}_{\min} \geq 15^{\circ}$
TA hotspot	$4.6 \leq \sigma_{\text{hotspot}} \leq 5.6$
Auger flux	$E_{231} \leq 57 \text{ EeV}$
Auger 2-point	$\mathcal{P}_{\min} \geq 10^{-3}$ for 3 out of 10 real.

Table 1: Summary of the criteria used to assess the compatibility of the simulated data sets with the Auger and TA data.

5.2. Results of the transient source scenarios

In this subsection, we show the results of the simulations obtained in the case of bursting sources. The reference source model is the GRB model described in Globus et al. (2015).

5.2.1. Reproducing the flux excess in the TA sky

In Fig. 3, we have shown the range of variations of the energy spectra in the case of our transient GRB source model with $B_{\text{EGMF}} = 0.1$ nG. As already discussed in Sect. 5.1.1, the Auger spectrum is easily reproduced by this model. On the other hand, the TA spectrum appears as a particularly strong upward fluctuation of the average all-sky flux. This can be naturally obtained with a very

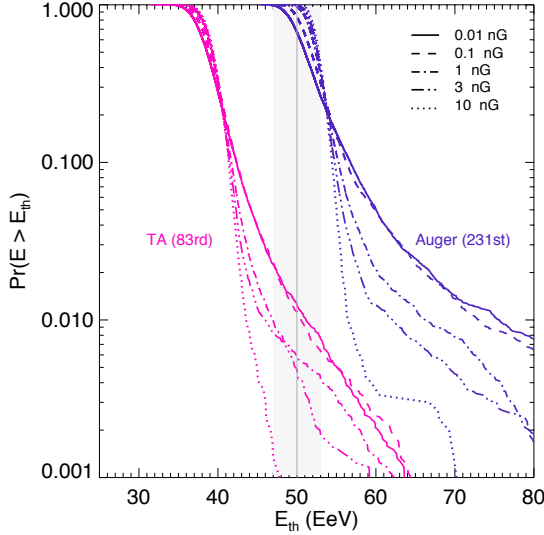


Fig. 5.— Cumulative probability distribution of the energy of the 83rd highest energy events in the simulated TA-like data sets, E_{83} (pink), and of the 231st highest energy events in the simulated Auger-like data sets, E_{231} (purple), for the transient source model with different values of the EGMF, as indicated. Shown is the probability that E_{83} and E_{231} are larger than the energy given in abscissa.

luminous source at high declinations in equatorial coordinates.

As discussed in Sect. 5.1.2, a simulated data set is declared similar to the TA data if $47 \leq E_{83}(\text{EeV}) \leq 53$. In Fig. 5, we show the cumulative probability distribution of E_{83} among all realisations of the transient source model. This is shown for four different values of the EGMF (pink lines). As expected, the value of E_{83} is usually much lower than the actual value for TA, namely 50 EeV. In 80% of the cases, the value of E_{83} is lower than 40 EeV, whatever the EGMF. However, a small fraction of the realisations can have a much larger value of E_{83} , which reflects the contribution of a nearby source providing a much larger number of events than average at high energy. This is all the more probable that the EGMF is low, because of the smaller time spread of the UHECRs reaching us from the source. The source is thus visible for a shorter amount of time, but its ap-

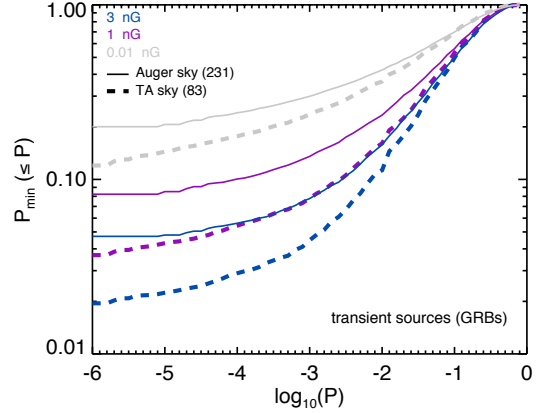


Fig. 6.— Cumulative probability distribution of the value of P_{\min} defined in Sect. 5.1.3, associated with the 2-point correlation function analysis. All curves correspond to the case of transient sources, with the three indicated values of the magnetic field (and a coherence length $\lambda_c = 0.2$ Mpc). The solid (resp. dashed) lines are for Auger-like (resp. TA-like) simulated data sets, with the 231 (resp. 83) most energetic events.

parent luminosity is then correspondingly larger.

As can be seen on Fig. 5, for values of the EGMF as large as 10 nG, it is extremely improbable that a source can have a large enough contribution in the TA sky to explain the observed excess in the UHECR flux. For an EGMF value of 1 nG (and a coherence length of 200 kpc; or for an EGMF of 0.45 nG and a coherence length of 1 Mpc), E_{83} can reach 50 EeV in a few per mille of the realisations. Finally, for EGMF values below 0.1 nG, the occurrence rate may reach around one percent.

On the same figure, we also plot the value of E_{231} for the Auger-like simulated data sets. As can be seen, the actual value of $E_{231} = 52$ EeV is quite common indeed since the median value of the E_{231} distribution varies from 51 to 53 depending on the assumed value of the EGMF.

5.2.2. Reproducing the TA anisotropy patterns

We now turn to the analysis of the data sets from the point of view of anisotropy. Fig. 6 shows the cumulative probability distribution of

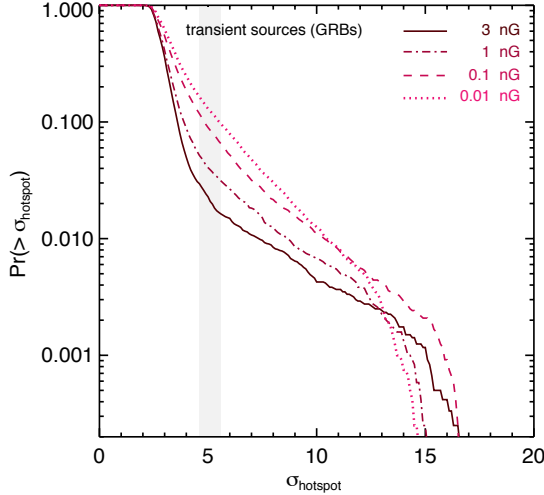


Fig. 7.— Cumulative probability distribution of the value of σ_{hotspot} defined in Sect. 5.1.3, associated with the clustering analysis with a 20° top-hat filter on the TA-like datasets simulated within the transient source scenario, for different values of the EGMF, as indicated.

the value of \mathcal{P}_{min} defined in Sect. 5.1.3, which allows us to compare the status of the simulated data sets with respect to the 2-point correlation function with that of the actual TA data set, for which $\mathcal{P}_{\text{min}} \simeq 10^{-3}$.

As can be seen, such a level of anisotropy in the TA sky is rather common if the EGMF is low: about 25% of the data sets have an anisotropy signal equal or larger to that of TA if $B_{\text{EGMF}} = 0.01$ nG (with $\lambda_c = 0.2$ Mpc). For larger magnetic fields, the probability is of course smaller. It is of the order of 8% for a 1 nG field, and of 5% for a 3 nG field.

On the other hand, Fig. 6 shows that much larger anisotropies are also possible, with occurrence rates not significantly lower than the previous ones. The probability for a data set to have $\mathcal{P}_{\text{min}} \leq 10^{-6}$ is only ~ 2 times lower than the probability to have $\mathcal{P}_{\text{min}} \leq 10^{-3}$. In other words, a large fraction of the anisotropic data sets are in fact *too* anisotropic to be compatible with the TA data, and must be rejected.

A similar conclusion can be reached from the study of clustering in the data sets, as indicated

in Sect. 4.2.3. In Fig. 7, we show the fraction of TA-like simulated data sets with σ_{hotspot} larger than a given value, as a function of that value, for different values of the EGMF. As can be seen, between $\sim 3\%$ of the data sets for a magnetic fields of 3 nG and $\sim 20\%$ of the data sets for a magnetic fields of 0.01 nG have a cluster of events with (unpenalised) significance larger than $\sigma_{\text{hotspot}} = 4.6$. However, among those, about 50% have in fact a significance larger than $\sigma_{\text{hotspot}} = 5.6$, and thus are incompatible with the TA data.

Now these data sets, like those with a too low value of \mathcal{P}_{min} , are typically those showing a very large contribution of one individual source, which raises an important and general problem: while flux excesses similar to that of TA can be obtained in a few percent of the realisations for low values of the EGMF (see above), it is very likely that these particular realisations are precisely those which give rise to too large an anisotropy. To investigate this, we now turn to the joint analysis of the two aspects, spectrum and anisotropy, of the simulated data sets.

5.2.3. Satisfying both spectrum and anisotropy constraints

The correlation between the number of events above 50 EeV and the maximum departure from isotropy revealed by the 2-point correlation function analysis is shown in Fig. 8. In this scatter plot, each dot corresponds to a TA-like simulated data set built from the transient source model, with N_{50} in abscissa and \mathcal{P}_{min} in ordinate, for 4 different values of the EGMF: 0.01 nG, 0.1 nG, 1 nG and 3 nG, all with a coherence length of 0.2 Mpc (see Sect. 4.1.1 for scaling). The position of the TA data set in this $\mathcal{P}_{\text{min}}-N_{50}$ plane is shown by the \odot symbol. The dashed area show the region where data sets are considered as passing the compatibility criteria of Sect. 5.1.

Unsurprisingly, most simulated datasets have much lower values of N_{50} , around 30–45, as would be the case in the actual TA data set if the TA spectrum were similar to that of Auger. It can also be seen that datasets with an acceptable value of \mathcal{P}_{min} are not uncommon. As a matter of fact, Fig. 6 corresponds to the projection of this scatter plot on the y-axis. Note that in order to evaluate \mathcal{P}_{min} , we computed one million random realisations of an isotropic flux. Therefore, we cannot

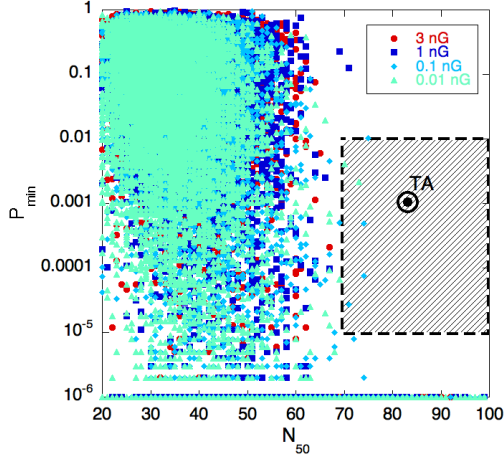


Fig. 8.— Scatter plot of the values of \mathcal{P}_{\min} vs. N_{50} for all the TA-like data sets simulated in the transient source scenarios, with 4 values of the EGMF, as indicated. The position of the actual TA data set is indicated by the \odot symbol, and the dashed area corresponds to the region where the data sets satisfy the “compatibility” criteria described in Sect. 5.1. Note that only the realisations fulfilling both the “Auger flux” and “Auger 2-point” criteria are considered in this scatter plot.

attribute values to \mathcal{P}_{\min} lower than 10^{-6} . The datasets corresponding to the dots on the x-axis line are datasets which, at one angular scale at least, are further away from the isotropic expectation than any of the simulated isotropic datasets. For these realisations, 10^{-6} is thus in fact an upper limit to their \mathcal{P}_{\min} value. As can be seen, data sets for which the value of N_{50} is large enough to be compatible with the TA spectrum do exist: they correspond to the small fraction of datasets with large values of E_{83} in Fig. 5. However, almost all of them have prohibitive values of \mathcal{P}_{\min} , due to the concentration of events from one very bright source, which is responsible for the flux excess. Only 5 data sets satisfy the relaxed criteria, with $\mathcal{P}_{\min} \geq 10^{-5}$, and only 3 the more strict criteria, with $\mathcal{P}_{\min} \geq 10^{-4}$, all with low values of the magnetic field, and all with values of N_{50} in the lower part of the selected range.

In Fig. 9, a similar plot is displayed, corresponding to the correlation between \mathcal{P}_{\min} and σ_{hotspot} ,

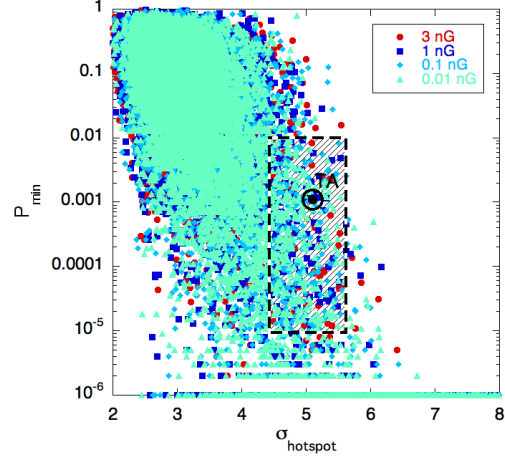


Fig. 9.— Same as Fig. 8, with the values of \mathcal{P}_{\min} vs. σ_{hotspot} , as defined in Sect. 5.1.

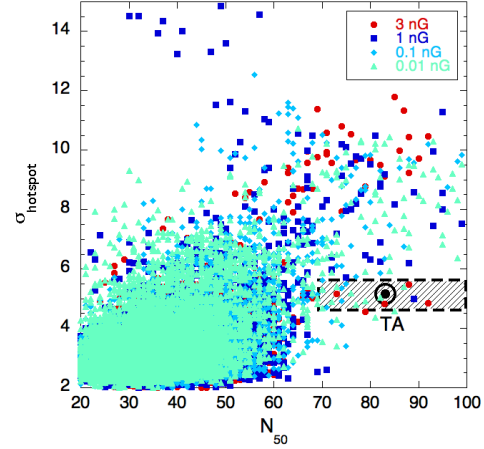


Fig. 10.— Same as Fig. 8, with the values of σ_{hotspot} vs. N_{50} .

as defined in Sect. 5.1. Although most data sets have a value of σ_{hotspot} between 2 and 4, a sizeable fraction of the data sets with an appropriate value of \mathcal{P}_{\min} show clustering properties compatible with the TA data, with σ_{hotspot} around 5, rather independently of the EGMF value.

A third correlation plot is shown in Fig. 10, comparing the clustering properties, estimated

B_{EG}	\mathcal{P}_{min}	σ_{hotspot}	N_{50}	$\mathcal{P}_{\text{min}} \ \& \ \sigma_{\text{hotspot}}$	$N_{50} \ \& \ \sigma_{\text{hotspot}}$	$N_{50} \ \& \ \mathcal{P}_{\text{min}}$	all
0.01 nG	0.06	0.04	0.004	0.007	0.0006	0	0
0.1 nG	0.05	0.03	0.003	0.008	0.0003	0.0002	0
1 nG	0.04	0.01	0.002	0.003	0	0	0
3 nG	0.03	0.01	0.002	0.003	0.0004	0	0

Table 2: Number of simulated data sets satisfying the various criteria and combinations of criteria of compatibility with the TA data, divided by the number of simulated data sets, in the transient source scenario. Each line correspond to a different assumption on the EGMF, as indicated. The title of the columns refer to the different criteria (see text and Table 1). Only the data sets which also satisfy the Auger criteria are indicated here. The number of simulated data sets is 12000.

through σ_{hotspot} , with the flux properties, estimated through N_{50} . Again, most data sets will large enough values of N_{50} to be potentially compatible with the TA spectrum have clusters with a much larger significance than the TA hotspot. The number of viable models, i.e. the number of points inside the compatibility dashed box, is larger than when putting together the N_{50} and \mathcal{P}_{min} constraints, and from this point of view, the clustering properties may be regarded as less constraining than the 2-point correlation function. Most of the data sets allowed by the σ_{hotspot} criterion are rejected for having a too low value of \mathcal{P}_{min} . However, the clustering criterion are not totally redundant, since some of the data sets allowed by the 2-point correlation function turn out to show too much clustering, sometimes at lower angular scales than observed.

A global summary of our study of the transient source scenario can be found in Table 2, which gives the number of simulated data sets satisfying the various “compatibility” criteria summarised in Table 1. The four lines of the table correspond to four different values of the EGMF, as indicated in the first column. In each case, a total of 12000 data sets were simulated. The numbers in the three following columns table give the number of TA-like simulated data sets satisfying independently each of the three criteria for TA, regarding the value of \mathcal{P}_{min} (2-point correlation function), the value of σ_{hotspot} (clustering analysis), and the value of N_{50} (high-energy flux). As already discussed, the most stringent constraint is by far the last one. The next three columns give the number of data sets satisfying jointly two of the three criteria, as indicated. Again, the combination of a high flux above 50 EeV and a relatively weak

anisotropy, as measured by the 2-point correlation function, is extremely rare. Only 2 data sets satisfy these conditions together. Finally, the last column gives the number of data sets satisfying all criteria. When this is done, as it turns out, none of the simulated data set survives.

Note that only the data sets which also satisfy the Auger criteria have been considered here (see Table 1). Note also that the requirement that the angular scale of the maximum departure from isotropy in the 2-point correlation function analysis be larger than 15° is implemented in the table, while it was not in the scatter plots of Fig. 8 and 9, which only show the value of \mathcal{P}_{min} . This explains why the numbers in the table may be smaller than the number of data sets appearing in the compatibility boxes of Figs. 8, 9 and 10.

As a conclusion, the transient source scenario does not appear to be a likely candidate to account for the currently available observational data, at least with the general assumptions inherent to our model.

5.3. Results of the steady source scenarios

We now turn to the case of steady sources. In this case, the propagation time delay of the particles and its spread have no direct incidence on the apparent luminosity of the source. However, the galactic and extragalactic magnetic fields play a role in spreading the UHECRs. We present here the results of extensive simulations of the steady source scenario with 4 values of the magnetic field, $B_{\text{EGMF}} = 0.1, 1, 3$ and 10 nG, and two different source densities: $n_s = 10^{-4}$ and 10^{-5} Mpc^{-3} .

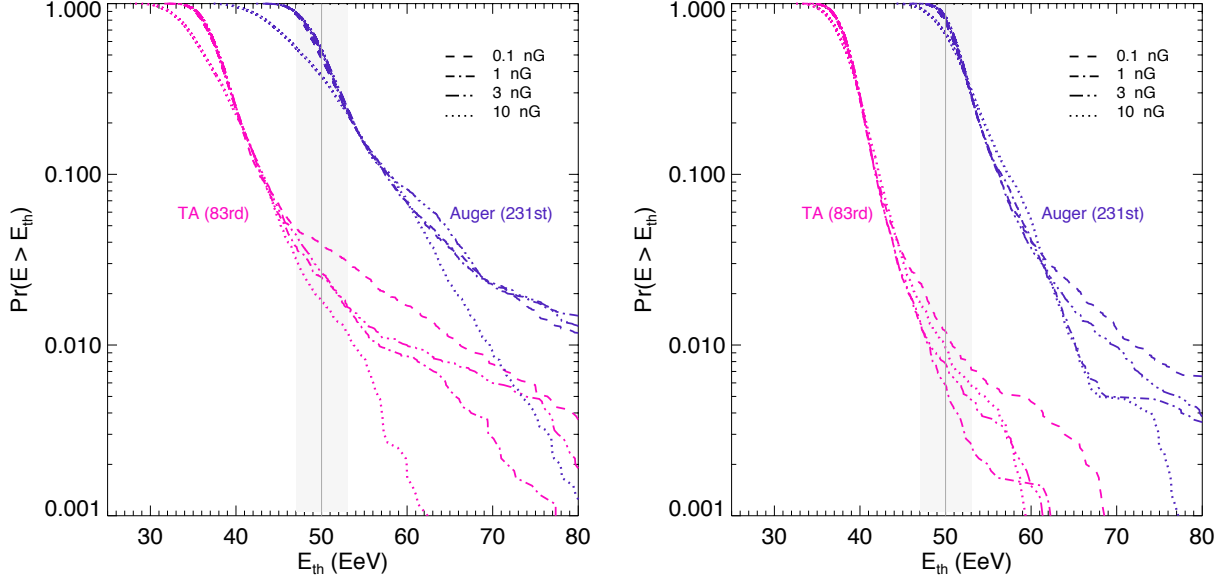


Fig. 11.— Cumulative probability distribution of the energy of the 83rd highest energy events in the simulated TA-like data sets, E_{83} (pink), and of the 231st highest energy events in the simulated Auger-like data sets, E_{231} (purple), for the steady source model with different values of the EGMF, as indicated. The left and right plots correspond to a source density of 10^{-5} Mpc^{-3} and 10^{-4} Mpc^{-3} respectively.

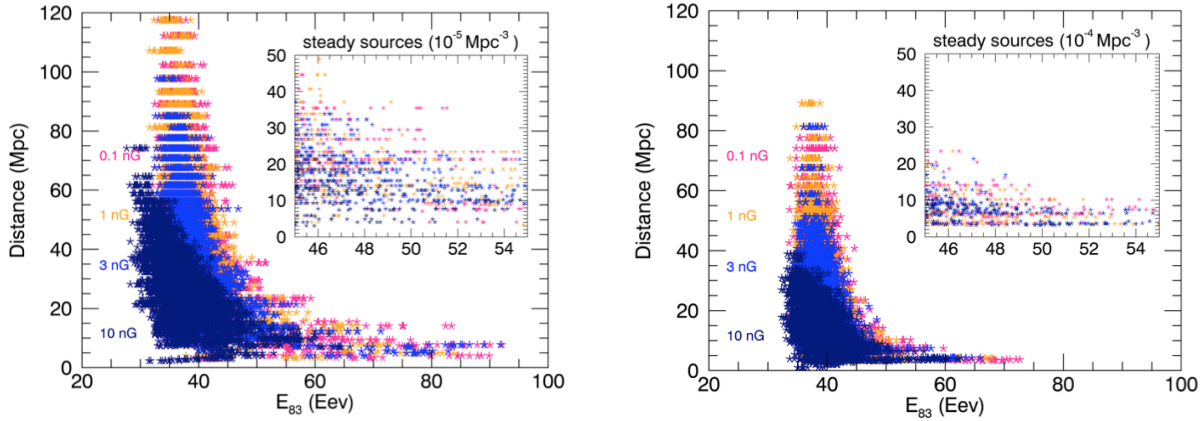


Fig. 12.— Scatter plot of the values of the source distance vs. E_{83} for all the TA-like data sets simulated in the steady source scenario, for a source density of 10^{-5} Mpc^{-3} (left) and 10^{-4} Mpc^{-3} (right), with 4 values of the magnetic field, as indicated. The data sets satisfy the TA “compatibility” criteria on the flux (described in Sect. 5.1) for $47 \leq E_{83}(\text{EeV}) \leq 53$. In that case the source distance is $\lesssim 20 \text{ Mpc}$ for a source density of 10^{-5} Mpc^{-3} and $\lesssim 10 \text{ Mpc}$ for a source density of 10^{-4} Mpc^{-3} .

5.3.1. Reproducing the flux excess in the TA sky

As in the case of transient sources, most of the simulated data sets have an energy spectrum com-

patible with the Auger spectrum. However, some realisations happen to have a particularly nearby and intense source in the Northern hemisphere, which can result in TA-like simulated data sets with a significantly higher flux at the highest energies. In order to assess the compatibility of our simulations with the observational data, we determine the energy of the 83rd highest energy event in the TA-like data set and of the 231st highest energy event in the Auger-like simulated data set, and compare them with the actual TA and Auger data. The fractions of simulated data sets with E_{83} and E_{231} larger than a given energy, E_{th} , are shown in Fig. 11, for different EGMF assumptions.

As can be seen, the requirement that the value of E_{231} in the Auger sky be not larger than 57 EeV is satisfied in all cases for $\simeq 90\%$ of the data sets. However, values of E_{83} in the TA sky larger than 47 EeV, corresponding to an excess of the high energy flux similar to that measured by TA, are relatively rare, especially in the case of larger source densities. For $n_s = 10^{-5} \text{ Mpc}^{-3}$, around 3% of the data sets satisfy the criterion, while this fraction drops to between 1% and 2% for $n_s = 10^{-4} \text{ Mpc}^{-3}$. As can be noted, this fraction does not depend much on the EGMF value, contrary to the transient source case where larger fields resulted in larger time spreads for the particles and thus weaker flux excesses. The effect of the EGMF is nevertheless visible for the lower source density, where the lower probabilities obtained for large magnetic fields (also visible in the part of the curve corresponding to low values of E_{th}) is due to the magnetic horizon effect, which attenuates the flux of UHECRs received from sources at intermediate distances.

Figure 12 shows the two scatter plots corresponding to the correlation between the source distance and E_{83} for the two source densities. We see that to obtain $47 \leq E_{83}(\text{EeV}) \leq 53$, the distance of the dominant source is $\lesssim 20$ Mpc for a source density of 10^{-5} Mpc^{-3} and $\lesssim 10$ Mpc for a source density of 10^{-4} Mpc^{-3} .

5.3.2. Reproducing the TA anisotropy patterns

As in the case of transient sources, essentially all the data sets with a large enough flux excess are characterised by a dominant source, whose presence in the sky is expected to result in a strong anisotropy, potentially incompatible with the ac-

tual data. To study this point, we first considered the 2-point correlation function of the simulated data sets, and computed the value of \mathcal{P}_{min} , as defined in Sect. 5.1.3. This corresponds to the probability that a data set built from an isotropic background be at least as anisotropic as the data set under study, at the angular scale where this probability is minimum. The results are shown in Fig. 13, where the probability for \mathcal{P}_{min} to be lower than a given value is represented as a function of that value.

We first note that the data sets built from an astrophysical model with a lower source density are more likely to exhibit large anisotropies, as was expected considering that fewer sources and contributing to the observed flux, so that the dominant source is more likely to contribute a large fraction of the UHECRs. Also expected is the influence of the magnetic field: larger values of the EGMF result in rarer occurrences of large anisotropies. According to our simulations, in the case of a source density $n_s = 10^{-5} \text{ Mpc}^{-3}$, around 12% of the TA-like data sets have a value of \mathcal{P}_{min} lower (and are thus more anisotropic) than the TA data set in the case of a 3 nG field, while this fraction rises up to 25% for a 0.1 nG field. These fractions are of the order of 8% and 12%, respectively, if the source density is $n_s = 10^{-4} \text{ Mpc}^{-3}$.

Although these numbers are reasonably large, Fig. 13 shows that much larger anisotropies are also fairly common. For these two values of the EGMF Between 3% and 12% of the TA-like simulated data sets have a value of \mathcal{P}_{min} as low as 10^{-6} , depending on the source density and EGMF. Now, as noted in the previous section for transient sources, these are the most likely to exhibit large flux excesses, so that most of the data sets satisfying one or the other of the flux and anisotropy criteria may have difficulties to satisfy both. This is further studied in the next subsection, where we combine several constraints.

The second anisotropy criterion relates to the clustering properties of the TA-like simulated data sets, through the value of σ_{hotspot} defined previously. The cumulative distribution of this quantity is shown in Fig. 14 for 4 different values of the magnetic field and the two different source densities. The compatibility range, between 4.6 and 5.6, is indicated by the grey area. As could be anticipated, the data sets corresponding to larger

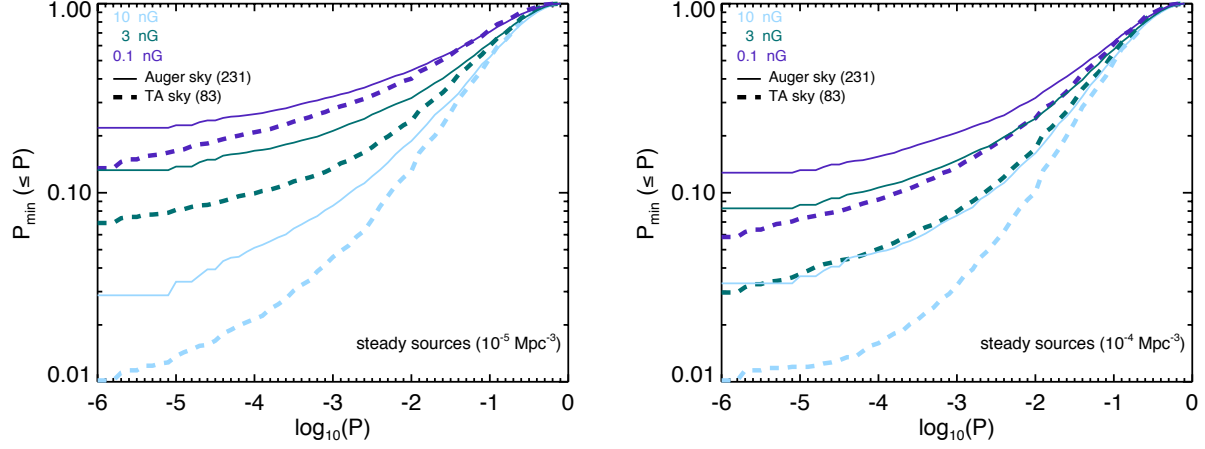


Fig. 13.— Cumulative probability distribution of the value of \mathcal{P}_{\min} defined in Sect. 5.1.3, associated with the 2-point correlation function analysis. All curves correspond to the case of steady sources, with the three indicated values of the magnetic field (and a coherence length $\lambda_c = 0.2$ Mpc). The solid (resp. dashed) lines are for Auger-like (resp. TA-like) simulated data sets, with the 231 (resp. 83) most energetic events. The left and right plots correspond to a source density of 10^{-5} Mpc^{-3} and 10^{-4} Mpc^{-3} respectively.

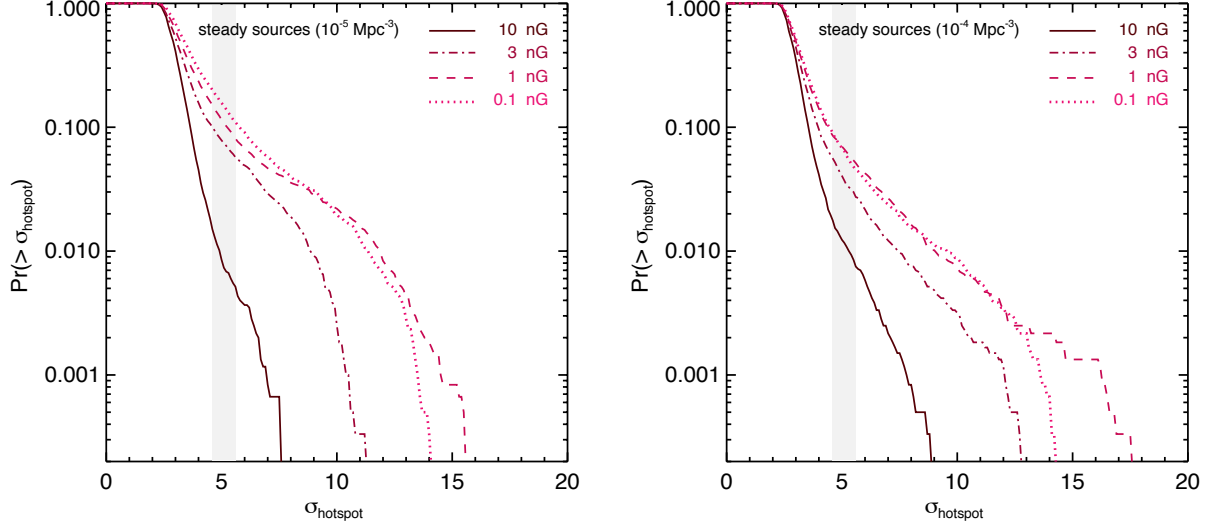


Fig. 14.— Cumulative probability distribution of the value of σ_{hotspot} defined in Sect. 5.1.3, associated with the clustering analysis with a 20° top-hat filter on the TA-like datasets simulated within the steady source scenario, for different values of the EGMF, as indicated. The grey area indicates the compatibility range.

values of the EGMF have a smaller probability to show a very large anisotropy. However, the influence of the source density can be seen to be rela-

tively moderated. This is reminiscent of the result of our simplified analytical study, where we found that the angular scale of the dominant source in

B_{EG}	\mathcal{P}_{min}		σ_{hotspot}		N_{50}		$\mathcal{P}_{\text{min}} \ \& \ \sigma_{\text{hs}}$		$N_{50} \ \& \ \sigma_{\text{hs}}$		$N_{50} \ \& \ \mathcal{P}_{\text{min}}$		all	
0.1 nG	0.08	0.06	0.06	0.03	0.003	0.008	0.01	0.006	0.0002	0.0007	0	0	0	0
1 nG	0.08	0.06	0.04	0.03	0.005	0.004	0.01	0.005	0.0003	0.0007	0.0002	0.0002	0	0
3 nG	0.07	0.06	0.03	0.02	0.01	0.003	0.008	0.006	0.0007	0.0003	0.0002	0.0005	0	0
10 nG	0.005	0.03	0.003	0.003	0.001	0.004	0.0008	0.001	0.0002	0.001	0.0008	0.002	0	0.0003

Table 3: Same as table 2, but for the steady source scenario. For each criterion or combination of criteria indicated in the first line, and for each value of the magnetic field indicated in the first column, we give the number of data set satisfying the criterion divided by the total number of simulated data sets (here 6000) corresponding to a source density $n_s = 10^{-5} \text{ Mpc}^{-3}$ (left columns) and to a source density $n_s = 10^{-4} \text{ Mpc}^{-3}$ (right columns).

the sky had a weak dependence in n_s , with a power 1/4 (see Eq. 15). Again, even though a few percent of the data sets have clustering properties compatible with that of the TA data, a substantial fraction of those have clusters which are in fact much more significant than the TA hotspot. Now these are the most likely to be the ones with a high flux excess above 50 EeV, as required by the TA spectrum.

The situation in the case of a 10 nG field is quite different, as can be seen in Fig. 13 and Fig. 14, the probability of observing a strong anisotropy decreases quite drastically passing from a 3 nG to a 10 nG EGMF. This is due to the fact that in the case of the largest field, the propagation time needed, say for a O nucleus at 50 EeV, to be isotropized is in average of the order of 100 Myr (see Globus, Allard, Parizot (2008)) while it takes approximately 10 times larger in the case of a 3 nG field. With such a large field, one thus enters a regime where the isotropization time of the highest energy nuclei becomes significantly shorter than their (time-)Horizon for energy losses (with is of the order of 100 Mpc/c for a 50 EeV O nucleus). In other words, for such a strong value of the EGMF, only UHECR nuclei coming from relatively nearby sources (well within the horizon) have a chance to reach the observer without being previously completely isotropized on their way. The more drastic condition for a UHE nucleus not to be isotropized on its way results in a significantly lower probability to get a strongly anisotropic sky. Interestingly, with such a lower probability of a strong anisotropy the 10 nG field case is the only case for which the probability to see much stronger anisotropy than what is seen in TA data is not significantly larger than the prob-

ability to see a flux excess compatible with the data, this is all the more true for the clustering properties.

5.3.3. Satisfying both spectrum and anisotropy constraints

The different elements to allows the combined analyses of the spectrum and anisotropy constraints for the steady case are reported in Table 3 and displayed in Figs. 15, 16 and 17. Before discussing the combined analyses, it is first useful to discuss the individual criteria and in particular N_{50} , the number of events above 50 EeV, reported in Table 3. We remind that both Table 3 and the scatter plots only take into account realisations which have passed both the Auger 2-point and Auger flux criteria (see Table. 1). The number which appear in Table 3 for the N_{50} criterion look at first in contradiction with Fig. 13 displaying the cumulative distribution of E_{83} , in particular in the case of the low density case (10^{-5} Mpc^{-3} and the lowest magnetic field case 0.1 nG. In that case, while the probability to obtain $E_{th} \geq 47 \text{ EeV}$ is of the order of 5%, only 15 dataset are reported to pass the N_{50} in Table 3. This apparent contradiction can however be understood considering that a majority ($\sim 2/3$) of the dataset showing a value of $E_{th} \geq 47 \text{ EeV}$ also have $E_{83} \geq 53 \text{ EeV}$ and thus do not pass the N_{50} criterion. Furthermore, it turns out that most of the realisations having a E_{83} in the appropriate range to fulfil the N_{50} criterion (and which thus are not among the 3% of the realisations showing the largest flux excess) are in fact due to sources located in sky region of relatively exposure for the TA observatory which are precisely the portions of the sky which are also visible for the Pierre Auger observatory. As

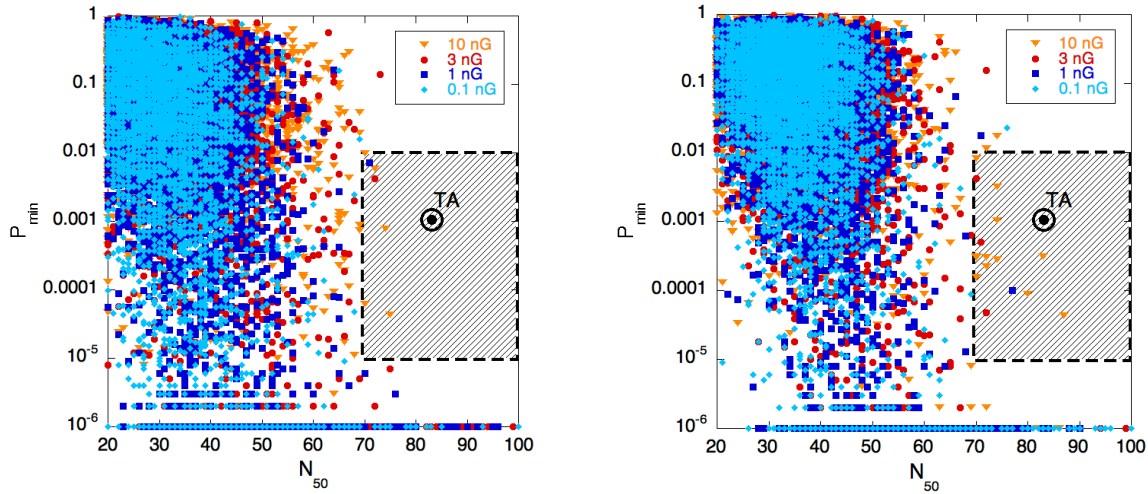


Fig. 15.— Scatter plot of the values of \mathcal{P}_{\min} vs. N_{50} for all the TA-like data sets simulated in the steady source scenario, for a source density of 10^{-5} Mpc^{-3} (left) and 10^{-4} Mpc^{-3} (right), with 4 values of the magnetic field, as indicated. The position of the actual TA data set is indicated by the \odot symbol. The dashed area corresponds to the region where the data sets satisfy the “compatibility” criteria described in Sect. 5.1.

a result most ($\sim 85\%$) of the datasets which are in the appropriate range of N_{50} in the low density and low magnetic field case also show strong anisotropies in the corresponding Auger datasets and are thus rejected by the Auger 2-point cut. The situation is less severe for the 1 nG and 3 nG cases. The flux attenuation due to larger value of the magnetic, makes the probability of obtaining large value of E_{83} or equivalently N_{50} lower and the value of N_{50} in the appropriate range are now mostly due to sources located in high exposure regions of the TA sky for which the overlap Auger is lower. The effect of the Auger 2-point cut is thus milder in the 1 nG case and all the more in the 3 nG case. For the latter moreover, even if the strongest source is located in the overlap between Auger and TA skies, the probability to be rejected by the Auger 2-point cut is significantly lower than for the lower fields. Finally, in the case of the 10 nG, still for the low density case, the strongest source distance is usually large enough so that its flux is highly deflected during the extragalactic propagation and thus visible in both hemispheres. For most datasets a large value of E_{83} also results in a large value of E_{231} and those

realisations are thus rejected by the Auger flux cut.

The different effects discussed above are much less severe for the largest density case (10^{-4} Mpc^{-3}). As can be seen in Fig. 13, the probability for a large value of E_{83} is lower than in the low density case and depend less on the value of the EGMP. The appropriate flux excesses are mostly due sources located in large exposure portions of the TA sky. The Auger 2-point cut is then less effective and rejects a lower fraction of the realisations. On the other hand in the 10 nG case, the larger density assumed leads to closer sources which means that their flux is less likely to be fully isotropized a trigger also a flux excess in the Auger sky. These elements partly explain why in the combined analysis of the spectrum and anisotropy we discuss in the next paragraphs the larger density case will turn out to be more favorable in the attempt of reproducing the observed data.

We now turn the correlation between N_{50} and \mathcal{P}_{\min} , show in Fig. 15. Each dot on the scatter plot corresponds to a TA-like simulated data set

built from the steady source model with a source density of $n_s = 10^{-4} \text{ Mpc}^{-3}$. Four different values of the magnetic field are superimposed, each with a specific colour. As in Fig. 8, the dashed area show the region where data sets are considered as passing the compatibility criteria of Sect. 5.1.

Similar comments as in the case of transient sources can be made. First, it is clear that most simulated data sets are very far from the compatibility region. They have much lower values of N_{50} , i.e. their integrated high energy flux is much lower, and their anisotropy is smaller. However a large subset of the simulated data sets have a two-point correlation function indicator, \mathcal{P}_{\min} , compatible with that of TA, as already shown in the previous subsection. But as can be seen, the vast majority of these data sets do not have any particular excess in the high-energy flux, and are thus incompatible with the TA data. On the other hand, there is a small fraction (see above) of the data sets which do have a large flux excess, but almost all of them exhibit a much larger anisotropy than the TA data, with values of \mathcal{P}_{\min} lower than 10^{-6} , all the more for the lowest values of the EGMF.

Nevertheless, a few data sets happen to satisfy both criteria at once mostly in the largest density case : 9 for an EGMF of 10 nG, 3 for an EGMF of 3 nG, 1 for an EGMF of 1 nG, and none for an EGMF of 0.1 nG (see Table 3). While quantitative conclusions cannot be drawn from such small number statistics, it does appear that larger magnetic fields are more favorable than lower ones. This is due to the larger angular spread, large magnetic fields are in fact required, to attenuate the anisotropy due to the most nearby source which would otherwise be too strong. In the case of lower magnetic fields, the realisations predicting a value of N_{50} in the appropriate range, result much too strong anisotropies, and the corresponding data sets are systematically much below the compatibility box in the scatter plot of Fig. 15. The situation worsens in the low density case, while their number is dramatically reduced by the Auger criteria, realisations passing the N_{50} almost systematically show very strong anisotropies.

In Figs. 16 and 17, we show the other two scatter plots corresponding to the correlation between \mathcal{P}_{\min} and σ_{hotspot} and between σ_{hotspot} and N_{50} , respectively, in the case of a source density of 10^{-4} Mpc^{-3} . As in the case of transient sources,

the clustering and 2-point correlation criteria are jointly satisfied only for a small subset of the data sets. As can be seen in Table 3, ~ 25 to 30 % of the realisations passing the σ_{hotspot} criterion also pass the \mathcal{P}_{\min} (the other being in most cases too anisotropic from the point of view of the 2-point analysis). Although this fraction is relatively large, it means that the two criteria are not redundant. As for the correlation between σ_{hotspot} and N_{50} , Fig. 17 shows that it tends to extend a bit more towards the compatibility region in the case of high magnetic fields. In particular, for low values of the EGMF, most of the data sets compatible with the TA flux excess above 50 EeV are much more strongly clustered than the TA data, with too large values of σ_{hotspot} (upper right part of the scatter plot). It also appears clearly again that high values of N_{50} are very uncommon, and that it is particularly difficult to satisfy the criterion on N_{50} together with an only moderate anisotropy (especially for low values of the EGMF).

Putting the flux and anisotropy criteria together, we see, for most combinaisons of the value of the source density and the EGMF, a very strong reduction of the number of acceptable data sets. Like in the case of transient sources, this is simply due to the fact that large excess in the flux require a very strong source, which is then very hard to “hide” in the anisotropy searches. Obviously, the best chance to reduce the excessive anisotropy is to increase the magnetic field. The number of acceptable data sets is thus largest for the 10 nG. In that case $\sim 1/3$ rd of the realisations passing the N_{50} criterion, also pass one of the two anisotropy criteria, this fraction appears to be much larger than in the lower magnetic field cases. Nevertheless, when requiring all three criteria together (plus the implicit criteria related to Auger), only 2 data sets remain, belonging to the same realisation of the steady source scenario with $n_s = 10^{-4} \text{ Mpc}^{-3}$ and $B_{\text{EG}} = 10 \text{ nG}$. The characteristics of such a realisation are shown and detailed in the Appendix 6.

6. Summary and discussion

In this paper, we have addressed the compatibility between the Auger and Telescope Array data on ultra-high energy cosmic rays. We first showed that, taken at face value, the two energy spectra

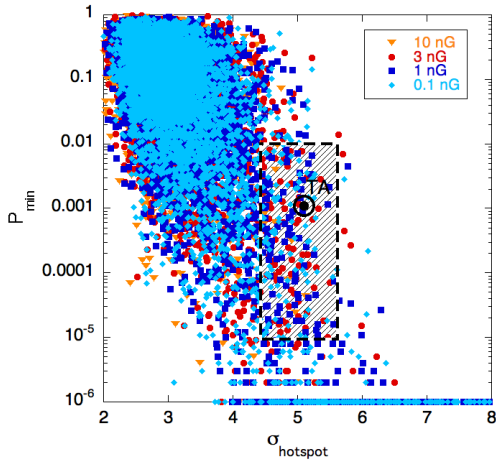


Fig. 16.— Same as Fig. 15, with the values of \mathcal{P}_{\min} vs. σ_{hotspot} , as defined in Sect. 5.1, for a steady source density of 10^{-4} Mpc^{-3} .

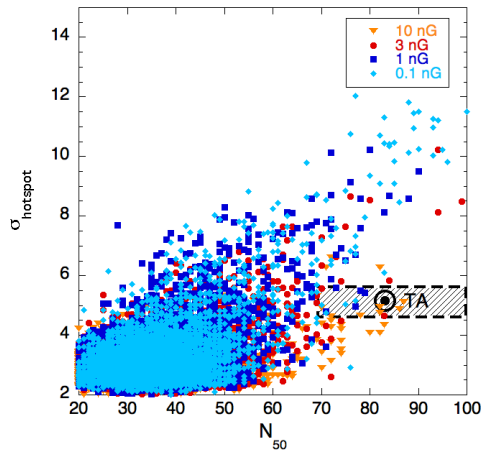


Fig. 17.— Same as Fig. 15, with the values of σ_{hotspot} vs. N_{50} , for a steady source density of 10^{-4} Mpc^{-3} .

don't appear to be mutually compatible. The TA spectrum cannot be considered a mere statistical fluctuation of the Auger spectrum, and vice versa, even if one allows for a global shift in the relative energy scale of the two experiments. In particular, the integrated flux measured by TA above 50 EeV

is significantly larger than that of Auger. This cannot be accounted for if the underlying UHECR flux is approximately the same in all direction, as the current anisotropy analyses reported by Auger suggests. However, the TA collaboration has reported a possible hotspot with an angular scale around 20° in the Northern hemisphere, in a part of the sky that is not observed by Auger. One may thus ask whether both features – a cluster of events and an excess in the flux at the highest energies – could be two complementary manifestations of a single reality: the presence of a very bright source in the Northern sky.

Assuming that the current Auger and TA data are indeed representative of the actual characteristics of the UHECRs in their respective parts of the sky, we investigated the possibility, for a given source model, to satisfy the various observational constraints. We considered a wide range of astrophysical scenarios, including transient sources or steading sources, as well as different source densities and different values of the EGMF.

Our simple analytic estimates show that such a flux excess could typically occur at most in a few percent of the cases, either in the transient source scenario or in the steady source scenario. However, the flux excess needed to account for the difference between the Auger and TA spectra corresponds to a number of events which is much larger than the number of events in the TA hotspot. We estimated that if the flux excess is to be explained by the contribution of one dominant source, that source should contribute around 45 ± 6 events in total, while the number of events in the so-called TA hotspot represents only $\sim 21\%$ of the total number of events including some possible background. Besides, it is striking that the highest energy events are not present in the hotspot region itself. In particular, in the initial report of the presence of an intermediate scale anisotropy in Abbasi et al. (2014), none of the 12 events observed by TA above 10^{20} eV (7 if the energy is rescaled downward by 13%) can be found within 20° of the hotspot center. This can be explained within our scenarios by simply noting that the rigidity of the highest energy particles is in fact smaller than those at intermediate energies, due to the change in composition. More specifically, CNO nuclei at 60 EeV have a rigidity twice as large as Fe nuclei at 100 EeV. The highest energy events might

thus very well (and are actually expected to) be deflected more than the particles between 50 and 60 EeV, say.

Our analytical estimates also suggested that the angular size of the hotspot associated to the flux excess is too small compared to the one observed by TA. In this respect, it is interesting to note that transient sources suffer from a general problem: larger deflections, as needed to fit the angular extension of the dominant source, also imply larger spreads in the particles arrival time, which in turn reduce the apparent flux of the source, and thus makes it even less likely for a source to contribute a large fraction of the total UHECR flux. Steady sources, on the other hand, do not suffer from this problem, since their apparent flux does not depend on the time spread of the particles, but only on its distance. Larger magnetic fields, at least in the direction of the source, might thus in principle increase its apparent angular size, without reducing its flux.

Our detailed simulations took into account the various effects influencing the propagation of the UHECRs, including energy losses, photodissociation in the case of nuclei, and deflections by the intervening magnetic fields, around the source, in the intergalactic medium and in the Galaxy. A remarkable feature that we noticed is that according to the representative model of the GMF by Jansson & Farrar (2012), UHECR propagation is significantly different in the Northern and Southern skies. The Galactic magnetic deflections are smaller at the North and hence the angular spreads and time delays are typically smaller for particles in the TA sky than in the Auger sky.

Our results are summarised in Tables 2 and 3. Overall, we find that transient sources are essentially incapable of reproducing the data. The steady source scenario does not appear *prima facie* to be very favorable either, with a probability $\sim 0.1\%$ to account for the reported data, because of the very low probability to have a strong, nearby source in the Northern sky. However steady sources are more likely than transients to account for data sets with general features reminiscent of the Auger and TA data. This difference between the two models arise because of the possibility to accept larger particle deflections, to attenuate the strong anisotropy usually produced by a strongly dominating source. Large values of the

EGMF are needed in this case. A clear requirement of such solutions is the necessity to have a very nearby source, within ~ 20 Mpc as can be inferred from Figure 12), in order to obtain a large flux excess in some part of the sky. Indeed such nearby sources such as M82 have been suggested as the origin of the TA hotspot (He et al. 2016; Pfeffer et al. 2016).

Concerning the underlying assumptions, the scenarios studied here rely on some generic features of the GRB source model developed in Globus et al. (2015). In particular, we used the same source composition and energy spectra, as well as the same distribution of relative luminosities at the sources. We argued and verified whenever possible that these specificities are not likely to modify significantly the conclusions of the study. Indeed, as far as the composition is concerned, it was shown previously to satisfy the current observational constraints derived from the Auger data. We note that an even heavier composition than the one we considered could in principle help attenuating the anisotropies, without reducing too much a possible flux excess in the TA sky, if the dominant source is far from the region of the sky observed by Auger, and most of its flux remains confined within the Northern equatorial hemisphere. Moreover, assuming that the composition is almost at its heaviest already at 50 EeV would make it more difficult to account for the fact that the highest energy events are not within the TA's hotspot while their number is also clearly in excess with respect to the Auger data. In the same line of reasoning, let us note that if the presence of a hotspot in TA dataset is confirmed with larger statistics, the study of the energy evolution of its significance will be critical in order to constrain the source composition and especially the presence of protons at lower energy. Indeed, Lemoine & Waxman (2009), pointed out that a cluster of events due to cosmic-rays nuclei with charge Z above an energy E , implies a clustering of UHECRs with the same rigidity but lower Z at the same spot. The statistical significance of the lower energy enhancement depends on the details of the source composition and spectra. We encourage the TA collaboration to search for such an enhancement and report on its existence or lack of.

Concerning the spectral shape at the source,

we do not expect other types of assumptions to modify strongly our conclusions, first because we did show that these allow to reproduce fairly well the Auger spectrum for the vast majority of the simulated data sets, which should probably be a common feature of most working scenarios, and second because we actually based our comparison with the data on the integrated spectrum above 50 EeV, which does not depend much on the actual shape of the high energy end of the spectrum. Finally, concerning the distribution of intrinsic luminosities among sources, it should be acknowledged that, as long as the UHECR sources are not known, and the acceleration process is not identified, one cannot make any reliable statement about it. We assumed the luminosity distribution resulting from the GRB source model. However, scenarios based on standard candles or on the contrary with a much wider luminosity distribution are in principle possible. From the point of view of producing a strongly dominating source, our assumptions lead a larger variance in the observed spectra than the standard candle scenario for a given inferred source density. Now, if the luminosity distribution were actually larger, it would increase the cosmic variance, with some realisations having their closest source particularly bright, or on the contrary only weak sources among the most nearby ones. This, however, would generally not produce an effect very different from what could be expected in the case of a lower source density, where fewer sources contributing a larger flux individually. To explore this, we also tested a source scenario with a source density of $n_s = 10^{-6} \text{ Mpc}^{-3}$, with 6000 additional data sets for two values of the extragalactic magnetic field. Less than 10 of those passed our flux criterion together with either of the two anisotropy criteria (2-point correlation function or clustering), but *none* passed the three criteria. In conclusion, we think that our results are relatively robust to possible changes in the astrophysical assumptions regarding the sources.

We note that the transient sources considered in this paper have been assumed to emit UHECRs isotropically, although a beamed emission is probable. As we pointed earlier the isotropic assumption adopted here is in fact optimistic in terms of the probability to produce a significant flux excess since beamed sources would be more numerous, have smaller intrinsic luminosities and any angu-

lar spreading in the vicinity of the sources would reduce the effective flux emitted in the direction of the observer, and thus reduce the probability of a large flux excess. Another specificity of our treatment of transient sources is that we applied an additional time delay in the propagation of the particles as if the sources were located in an environment similar to the that of the Sun, assuming a host galaxy with magnetic properties like ours. In principle, the source might be located in a strongly magnetized environment. This would further reduce the possibility to observe a large flux excess in the case of transient sources, by implying yet additional time delays. If these time delays are long enough, it may even turn transient sources into steady sources. This possibility appears extremely unlikely in a galactic magnetic environment similar to ours (at least with the Galactic magnetic field model we used throughout our study) because the typical GRB rate per galaxy ($\sim 10^{-5} \text{ yr}^{-1}$, assuming a beaming factor $f \simeq 100$) is too low for the ultra-high-energy cosmic-ray signal of different GRBs to significantly overlap in time. Starburst galaxies which are known to harbor much stronger magnetic fields than our own Galaxy (see for instance Beck (2015) for a review) may appear as a better candidate for such an overlap between successive GRBs to take place. Let us note however that this possibility remains at present speculative, since there is no strong established connexion between starburst galaxies and GRB explosion in the local universe (see Japelj et al. (2016); Vergani et al. (2016) for recent accounts).

Finally, from the point of view of the energy scale, we chose to rescale TA energy scale downward by 13% while we could have equivalently chosen to rescale Auger energy scale upward by the same amount. This choice was dictated both by the fact that Auger claimed systematic on the energy scale (14%) is lower than that of TA (22%) and also because at this energy scale the experimental value of $E_{231} = 52 \text{ EeV}$ corresponds quite closely the median value found in our simulations for most of our hypotheses on the extragalactic magnetic field, the rate or density of the sources. By choosing to rescale Auger energy scale by 13% upward we would thus have discussed the excess of events in TA dataset above 57 EeV rather than above 50 EeV. While it intuitively obvious that

the cosmic variance (and as a result the probability to observe a significant difference between TA and Auger number of events) is expected to increase with the energy, this effect should be quantitatively minor for a 13% shift in energy, all the more in the case of a composition getting heavier in this energy range. As soon as it remains moderate a global shift of the energy scale should thus not affect significantly our conclusions and appear to be much less relevant than energy dependent systematic errors for our present discussion. Since it is precisely the conjunction between a large flux excess and a moderate anisotropy (the latter being reproduced in $\sim 1\%$ of the simulated data sets) in the northern hemisphere which turned out to be particularly challenging to account for, the discovery of any energy dependent systematic effect allowing to reduce the high energy flux difference between the two hemispheres would alleviate the constraints imposed by current observations.

As conclusion, based on the results presented in this paper, it may be considered likely that the current features of the Auger and TA data, if confirmed by future observations, may either point towards rather unconventional astrophysical scenarios, or to a very particular situation in the universe, where we happen to be very close to an intense steady source, affected by particularly large magnetic deflections. Additional data, especially with reduced or “homogeneous” systematic uncertainties, allowing for a direct comparison between the Northern and Southern sky, with similar statistics, would definitely be of great help to address this issue. This could be provided by a space-based experiment like envisioned by the JEM-EUSO collaboration (Adams et al. 2014).

Acknowledgements

We thank Reiner Beck for very useful comments about the Galactic magnetic field. NG thanks David Eichler for inspiring discussions about ultra-high energy cosmic rays for more than a year. DA, CL and EP are indebted to Benjamin Rouillé d’Orfeuil for important contributions to the initial version of the sky map drawing procedure and analysis. We also thank greatly Hiroyuki Sagawa for providing important precisions about the Telescope Array data sets. This research was supported by I-Core CHE-ISF center of excellence of

research in astrophysics and by an Israel Space Agency grant (NG & TP), by the Lady Davis foundation (NG), and by the UnivEarthS Labex program at Sorbonne Paris Cité (ANR-10-LABX-0023 and ANR-11-IDEX-0005-02) (CL).

Simulated data set compatible with both TA and Auger

As can be seen on Fig. 18, the working realisation has distinctly different spectra in the Auger sky and in the TA sky, both very similar to those of the actual data. Essentially each of the 10 data sets simulated from this realisation have a suitable spectrum, with values of N_{50} which are all between 70 and 87, except one, which has $N_{50} = 67$. The average value is 74.

Regarding the criterion on \mathcal{P}_{\min} , we show in Fig. 19 the 2-point correlation functions of the 10 data sets of the realisation. All the Auger-like data sets (right panel) are seen to be compatible with isotropy, in agreement with the Auger data. As for the TA-like data sets (left panel), in 4 cases out of 10, the 2-point correlation function is very similar to that of TA (represented by the dashed line). Another one is also similar, but with lower probabilities at small angles. A sixth one may be considered marginally compatible, while the last 4 are clearly too much anisotropic.

Finally, Fig. 20 shows the sky maps corresponding to one of the two data sets satisfying all criteria, namely sample 9. It has the following values of the parameters: $N_{50} = 87$, $\sigma_{\text{hotspot}} = 5.1$, and $\mathcal{P}_{\min} = 4 \cdot 10^{-5}$. The color code in the figure allows us to identify the events coming from the same source. As can be seen, in the TA-like sky map (top panel) 59 events are coming from one single source, located at a distance of 6 Mpc, with a luminosity in cosmic rays above 10^{18} eV of $\sim 3 \cdot 10^{41}$ erg.s $^{-1}$. The anisotropy of this data set remains however moderate, mostly thanks to the large value of the EGMF, with events spreading over the whole sky. The second most intense source only contributes 7 of the 83 highest energy events, also distributed all over the map. Although the Auger-like sky map (lower panel) looks indeed compatible with isotropy (as was indicated by the 2-point correlation function), it is interesting to note that the dominant source in the TA sky is also vastly dominant in the Auger sky, contributing no less than 124 of the 231 highest energy events. However, these events are indeed spread throughout the whole sky, so the anisotropy remains essentially negligible. It should also be noted that the second most intense source in this Auger-like data set only contributes 22 events. This explains why the largely dominant source, visible in both hemispheres, is not leading to a UHECR flux that is too large compared with the high-energy flux measured by Auger. In other words, this particular realisation of the model actually corresponds to an otherwise downward fluctuation of the flux in the Auger-like sky, compensated by the large contribution of the most intense source in the sky to the overall flux in all directions.

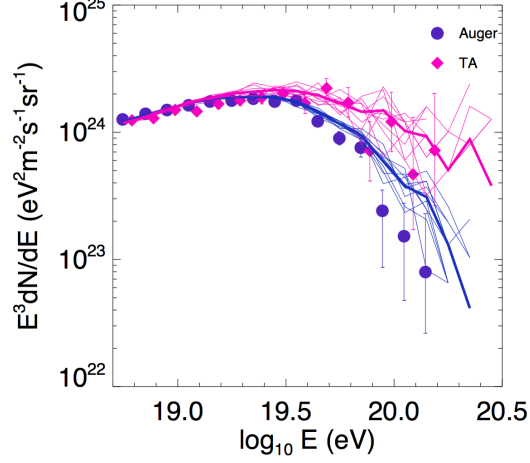


Fig. 18.— Spectra of the 10 data sets (thin lines) built from a realisation of the steady source scenario (with a source 10^{-4} Mpc^{-3} and an EGMF of 10 nG) which jointly satisfies the spectrum and anisotropy criteria of compatibility with the observations, together with the Auger and TA data points. The thick lines correspond to the average spectra of the 10 data sets. Note that even in this rare favorable case the expected average Auger spectrum is more than one sigma above the three highest observed points and none of the ten data sets actually paths below them.

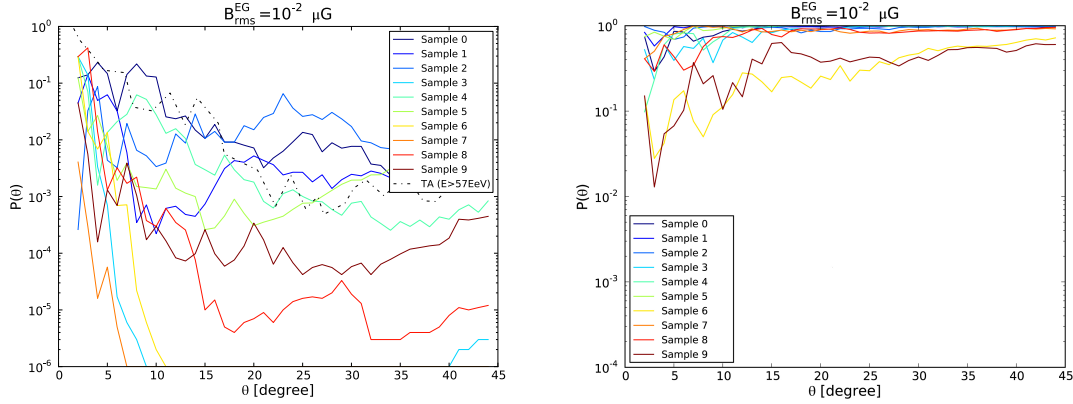


Fig. 19.— Two-point correlation functions of the 10 data sets obtained with the only realisation of the steady source scenarios which jointly satisfies the spectrum and anisotropy criteria of compatibility with the actual data (see text). Left: TA-like simulated data sets. The dashed line shows the 2-point correlation function of the actual TA data. Right: Auger-like simulated data sets.

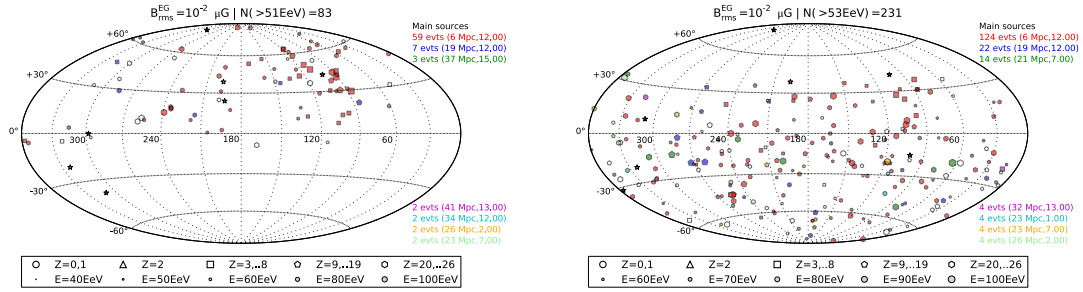


Fig. 20.— TA-like (left) and Auger-like (right) sky maps, in equatorial coordinates, corresponding to sample 9 of the steady source realisation shown in Figs. 18 and 19.

REFERENCES

- Aab, A. et al. (Pierre Auger Collaboration), 2014, Phys. Rev. D 90, 122005.
- Aab, A. et al. (Pierre Auger Collaboration), 2014, Phys. Rev. D 90, 122006.
- Aab A. [Pierre Auger Collaboration] The Pierre Auger Observatory: Contributions to the 34th International Cosmic Ray Conference, Proc. 34th ICRC, The Hague, The Netherlands
- Abbasi, R. U et al., The Astrophysical Journal Letters, 790:L21 (5pp), 2014 August 1
- Abraham, J. et al. (Pierre Auger Collaboration), 2004, Nucl. Instrum. Methods Phys. Res., Sect. A 523 50.
- Adams, J. H. (JEM-EUSO collaboration), 2014, Experimental Astronomy, Volume 40, Issue 1, pp.3-17
- Allard, D., Parizot, E., Olinto, A. V., Khan, E., & Goriely, S. 2005, A&A, 443, L29
- Beck, R., 2008, AIPC, 1085, 83
- Beck, R., 2009, Ap&SS, 320, 77
- Beck, R., 2015, Magnetic Fields in Spiral Galaxies, arXiv:1509.04522v4
- Blaksley, C.; Parizot, E.; Decerprit, G.; Allard, D., 2013, A&A, 552, 125
- Frail, D. A., Kulkarni, S. R., Sari, R., et al. 2001, ApJ, 522, L55
- Giacalone J., Jokipii J. R., 1999, ApJ, 520, 204
- Globus, N., Allard, D., Parizot, E., 2008, A&A, 479, 97
- Globus, N., Allard, D., Mochkovitch, R., and Parizot, E., 2015, MNRAS, 451, 5270
- Globus, N., Allard, D., Parizot, E., 2015, Phys. Rev. D Rapid. Com. 92, 021302
- Harari, D., Mollerach, S., & Roulet, E. 1999, J. High Energy Phys., 08, 022
- He H. , Kusenko A., Nagataki S., et al., 2016, Phys.Rev. D93, 043011
- Jansson, R. & Farrar, G. R., 2012, ApJ, 757, 14
- Japelj, J. et al., 2016, A&A 590, A129
- Kaway, H. et al. (Telescope Array Collaboration), 2008, NuclearPhysics B - Proceedings Supplements, 175 221.
- Komossa S., Journal of High Energy Astrophysics, Volume 7, September 2015, Pages 148?157
- Krause, M., 2007, MmSAI, 78, 314
- Lemoine, M. & Waxman, E., 2009, Journal of Cosmology and Astroparticle Physics, Issue 11, id. 009.
- Li, T.-P., & Ma, Y.-Q. 1983, ApJ, 272, 317
- Matthews J. [Telescope Array Collaboration] Highlights from The Telescope Array, 2015
- Pfeffer, D.N., Kovetz E.D., Kamionkowski M., <https://arxiv.org/abs/1512.04959>
- Rouillé d’Orfeuil, B.; Allard, D.; Lachaud, C.; Parizot, E.; Blaksley, C.; Nagataki, S., 2014, A&A, 567, 81
- Shaham N., Piran S., 2013, PhRvL, 110, 1101
- Takami, H. & Murase K., 2012, ApJ, 748, 9
- Tinyakov, P. et al (Telescope Array Collaboration), 2014, Nuclear Instruments and Methods in Physics Research A 742, 29D 34
- Tinyakov P [Telescope Array Collaboration] 2015, TA anisotropy summary, Proc. 34th ICRC, The Hague, The Netherlands.
- Unger M. [Pierre Auger and Telescope Array Collaborations] 2015 Report of the Working Group on the Composition of Ultra-High Energy Cosmic Rays, Proc. 34th ICRC, The Hague, The Netherlands.
- Vergani, S.et al., 2016, A&A 581, A102
- Wanderman D., Piran T., 2010, MNRAS, 406, 1944
- Waxman E., Miralda-Escude J., 1996, ApJ, 472, 89

This 2-column preprint was prepared with the AAS L^AT_EX macros v5.2.